Review

Towards a Glass New World: The Role of Ion-Exchange in Modern Technology

Simone Berneschi, Giancarlo C. Righini and Stefano Pelli *

"Nello Carrara" Institute of Applied Physics, IFAC-CNR, via Madonna del Piano 10, I-50019 Firenze, Italy; s.berneschi@ifac.cnr.it (S.B.); g.c.righini@ifac.cnr.it (G.C.R.)
* Correspondence: s.pelli@ifac.cnr.it; Tel.: +39-055-522-6393

Abstract: Glasses, in their different forms and compositions, have special properties that are not found in other materials. The combination of transparency and hardness at room temperature, combined with a suitable mechanical strength and excellent chemical durability, makes this material indispensable for many applications in different technological fields (as, for instance, the optical fibres which constitute the physical carrier for high-speed communication networks as well as the transducer for a wide range of high-performance sensors). For its part, ion-exchange from molten salts is a well-established, low-cost technology capable of modifying the chemical-physical properties of glass. The synergy between ion-exchange and glass has always been a happy marriage, from its ancient historical background for the realisation of wonderful artefacts, to the discovery of novel and fascinating solutions for modern technology (e.g., integrated optics). Getting inspiration from some hot topics related to the application context of this technique, the goal of this critical review is to show how ion-exchange in glass, far from being an obsolete process, can still have an important impact in everyday life, both at a merely commercial level as well as at that of frontier research.

1. Introduction

To celebrate, over time, the wedding anniversary between ion-exchange and glass, all noble metals (e.g., silver, gold, platinum, etc.) and gemstones (e.g., sapphire, emerald, diamond, etc.) offered by our generous planet would not be enough! In fact, the origin of this lucky marriage is lost in the dawn of time. The art of ancient glassmakers can be traced back to the 3rd millennium BC among the peoples of Egypt and the Middle East where the main raw material, the silica rich sand, was widely available. From there, this knowledge was transferred to the peoples of the Mediterranean Sea, including the Greeks and the Romans (see, for instance, the natron glass used during the Roman Empire period). Over these three millennia, the colouring of glass was given directly during its manufacture by introducing additive metal oxides, such as iron, copper, manganese, etc., to the raw materials before firing the whole system in a kiln and then cooling it in order to obtain the final product [1,2].

Only between the 6th and 7th centuries AD, the Egyptians began to use silver or copper pigments—in the form of powders—to decorate and colour the surface of their artefacts, such as dishes, vessels and pots, by means of a thermal annealing process in a furnace. Through this technique, the pigment became part of the atomic structure of the products, colouring them in correspondence of their surface. However, due to the low temperature of the firing process and the difficulty of controlling it, the final artefacts remained rather opaque [3,4]. Later, around the 9th century AD, this staining method—improved in terms of technological process (i.e., higher operating temperature; better kiln

performance) and now capable of giving glass lustre to ceramic artefacts—found great diffusion among the Mesopotamian peoples before arriving in Spain, in the first centuries of the millennium, following the expansion of Islamic culture [5,6]. In Europe, ion-exchange experienced a notable application during the outbreak of Gothic architecture (between 12th and 14th century) contributing to the realisation of the wonderful multi-coloured stained-glass windows of the cathedrals of that period. A paste, composed of clay/ochre and silver chloride/sulphide, was spread on the glass to be treated in order to produce a thin layer on its surface. Subsequently, the whole system was fired in a reducing atmosphere—induced in the furnace by introducing smoking substances—at a temperature close to the softening point of the glass. In these conditions, the ion-exchange process was triggered: the silver ions diffused inside the glass replacing the alkaline ions, such as sodium, widely present in the pristine glass. Finally, the simultaneous presence of reducing elements, both external (i.e., the smoking elements in the atmosphere) and internal to the glass (i.e., impurities, such as iron or arsenic), favoured the formation of silver metal nanoparticles (NPs) inside the ion-exchanged specimen, leading to a yellow-amber colour whose tonality and intensity depending on the process parameters (i.e., time and temperature) and the size of the NPs thus formed (from a few to one hundred nanometres), respectively. Other colours, such as red or green, were obtained using iron and copper salts, respectively. In the following renaissance period, this decorative technique became particularly popular in Italy in the creation of polychrome and lustre pottery artefacts, among which those of Deruta stood out par excellence [5,7].

It was only around the beginning of the 20th century that the foundations for a possible application of the ion-exchange process in the technical-industrial field were laid. In 1913 G. Schultze was the first to study the diffusion of silver ions into the glass using silver nitrate salt ($AgNO_3$) as ion source, starting a whole series of studies aimed to understand the chemical-physical nature of the phenomenon and its effects on some physical properties of the glass so treated. In particular, a few years later, in 1918 at the Schott Glass Laboratory, it was demonstrated that ion-exchange produces an increase of the refractive index of the layer of the glass involved in the diffusive process [4,8]. Only from the 1960s, however, the ion-exchange technique became an industrial standard process.

Among all the possible applications, glass strengthening represented the first example of glass modification by this standardized technique. The process was initially investigated in 1962 by S. S. Kistler and P. Acloque (the latter in collaboration with J. Tochon) who, in their works, demonstrated how the in-diffusion of ions having different atomic size in the pristine glass matrix (i.e., larger potassium ions K^+, originally present in the molten salt KNO_3, in place of smaller sodium ions Na^+ in the glass) was able to prevent or heal over the possible formation of micro/nano-cracks on the specimen surface, increasing its mechanical strength [9,10]. Since then, many efforts have been carried out until our days in this field both at research and industrial levels, and the development is still under way with amazing perspectives [10–13].

Almost simultaneously to glass strengthening, another key application of ion-exchange technique quickly began to establish itself. In fact, at the turn of '60s and '70s, the availability of the first optical fibres by Corning Inc (Corning, NY, USA), joined with the revolutionary vision of Bell Laboratories researchers J.E. Miller and colleagues, led to the aim of miniaturizing and integrating all necessary components for the generation, addressing, processing and detection of an optical signal on a single chip by means of optical waveguides and gave the decisive impulse for the development of integrated optics (IO). The ion-exchange process in glass greatly contributed to achieving these results [14–17]. Pioneering works in this field were given by T. Izawa and co-workers and T. G. Giallorenzi et al., at the beginning of the 1970s, who demonstrated the feasibility to obtain planar glass waveguides by thermal or field assisted ion-exchange using different molten salts, thus opening up the way for further development of novel integrated devices in the optical communications field [18,19]. Optical waveguides in glass by ion-exchange technique offered several advantages in comparison with other fabrication methods and materials: compatibility with

optical fibres, low propagation and coupling losses, low birefringence, low cost in terms of material and fabrication process, high stability and reliability. All these features contributed in the following decades to the boom of IO devices with different functionalities, such as passive (e.g., for signal addressing and processing), active (e.g., for signal generation or amplification, thanks to rare earths doping), or even hybrid, when both functionalities coexist in a same chip [20–39].

The third noteworthy application of ion-exchange was historically linked to the glass staining technique by the introduction of metal ions inside the pristine amorphous matrix during the process or, more frequently, by inducing their subsequent reduction into metallic form through an ad-hoc thermal post-process [40,41]. However, this approach of loading glass with metal ions or nanoparticles has been shown to go far beyond the mere colouring of the material. In fact, around the last decade of the 20th century, the progress in plasmonics—with the possibility to obtain both strong local field enhancement and high absorption cross-section by means of the surface plasmon resonance phenomenon in ion-exchanged dielectric substrates with embedded metal nanoparticles—has rapidly increased the research interest for these nanostructured materials [42–47], broadening their application horizon.

For instance, it was demonstrated that in ion-exchanged glasses the presence of noble metal nanoparticles (e.g., Au, Ag, or Cu), with their large third-order nonlinear susceptibility and ultrafast response, makes these materials suitable for applications also in non-linear optics [48–53].

Moreover, these embedded noble metal ions and nanoparticles played—and still do—an important role in the luminescence properties of the same ion-exchanged host materials especially when these are doped with elements belonging to the rare earth group, mitigating the limitation imposed on their concentration due to the occurrence of quenching phenomena. From the early works of Malta et al. [54] and Hayakawa et al. [55], the research literature on this topic has highlighted different reasons concerning the origin of the rare earth luminescence enhancement in optical glasses chemically treated by ion-exchange, depending on the nanostructure sizes so realized: (i) an energy transfer (ET) process between the energy levels of the noble metal ions (such as isolated Ag^+, Ag^+ - Ag^+ pairs or silver aggregates) and those belonging to rare earths ions; (ii) an ET mechanism among non-plasmonic small metal nanoparticles (i.e., molecule-like nanoparticles having few nanometres size) and the doping active elements; (iii) a local field enhancement around the rare earth ions due to the surface plasmon resonance (SPR) phenomenon induced in small metal nanoparticles [54–66]. In the technological field, the aforementioned mechanisms—together with the down/up-conversion ones—have favoured the use of these ion-exchange glass systems in the photovoltaic sector in order to increase the solar cell efficiency through tailored cover-glasses and in the development of low cost and high performance white/coloured solid-state light sources [67–81].

On the other hand, in sensing/biosensing applications, low-loss ion-exchanged planar waveguides with embedded metal ions represented the core of integrated optical sensors for the analytical determination of biomolecules at the interfaces by an evanescent wave interrogation mechanism, exploiting different optical detection approaches such as those based on fluorescence or absorption [82–90]. Furthermore, these ion-exchange optical waveguides have been used as excitation systems for surface plasmon resonance (SPR) or localized surface plasmon resonance (LSPR) in noble metal thin films or NP arrays selectively deposited on them. This approach replaced the more traditional Kretschmann configuration based on prism coupling and contributed to the realisation of hybrid-plasmonic label-free integrated optical biosensors with high performance [91–94]. Alternatively, the same noble NPs can be directly grown in the guiding structure in order to obtain LSPR optical waveguides for the detection of selected analytes by monitoring the changes in absorption spectra as a result of the chemical reaction occurred at the interface [95]. Last but not least, the possibility of making optical waveguides in one-dimensional (1D) or two-dimensional (2D) geometry with embedded noble metal nanoparticles, starting from

glass substrate by means of ion-exchange technique and an ad-hoc thermal post-process, has contributed in the last decades to the strong development of planar platforms for sensing/biosensing applications based on surface enhanced raman scattering (SERS) mechanism [96–104]. In comparison to the chemical procedures commonly adopted to bind metal NPs to the surface of a sample, the ion-exchange technique followed by a suitable thermal post-process represents a simpler and less expensive method for the manufacture of SERS substrates and provides the not negligible advantage of long-term stability of the metal nanoparticles thanks to their embedding within the same glass specimen [105–107].

From this wide range of scenarios, getting inspiration from some hot topics related to the application context of this technique, the goal of this critical review is to show how ion-exchange on glass, far from being an obsolete process, can still have an important impact in the everyday life, both at a merely commercial level as well as at that of frontier research.

2. Glass Strengthening: The Ion-Exchange Contribution

Today, it has become a cliché to associate the idea of glass with that of brittleness, so that, in the course of daily speaking, it is common to use the expression "fragile as glass" whenever one refers to an object destined to easily break. In this regard, Tennessee Williams, one of the most popular American playwrights, expresses himself in these terms about glass: "When you look at a piece of delicately spun glass you think of two things: how beautiful it is and how easily it can be broken" [108]. Moreover, the idea of brittleness associated with glass is so rooted in our mind that it stands as symbol of the uncertainty of life and the human condition as expressed by G. K. Chesterton in one of his aphorisms: "I felt and feel that life itself is as bright as the diamond, but as brittle as the window-pane" [109].

Yet, in spite of these beliefs, a pristine glass can tolerate high stresses, of the order of GPa. This makes glass an extremely strong material in itself [11–13,110]. A classic example is given by an optical fibre which, despite its size as thin as a hair, can achieve extraordinary mechanical tensile strengths (~few GPa) [111].

So, what does determine glass brittleness? The answer lies in the presence on its surface of microscale flaws occurring during the different steps of its manufacturing, processing and handling. Consequently, glass strength is drastically reduced by several orders of magnitude, down to only a few tens of MPa before reaching breaking point, once a mechanical stress is applied to its surface. If fused silica glass, thanks to its intrinsic structure, presents the best characteristics in terms of hardness and mechanical strength, multicomponent oxide glasses, such as soda-lime or float ones, are among the most produced due to their low cost and easier fabrication. However, due to their highly heterogeneous composition, they are more liable to the formation of surface defects during their processing and, therefore, more prone to breakage once they are subjected to mechanical stress. Unlike crystals which have a well-ordered internal atomic structure, glasses are characterized by a disordered and chaotic molecular configuration typical of the amorphous materials. The absence of a crystal lattice leads to the formation of shear bands in the material. From the observation of these bands that occurred in a metallic glass following their manufacturing process, A. Wisitsorasak and P. Wolynes developed a general theory capable of explaining how the breaking phenomenon occurs in these materials [112]. The model provides a mapping of all the possible configurations of the molecules in the solid, in order to describe how the mechanical stress changes the atomic rearrangement rate in the glassy material, with the consequent formation of the shear bands. The observation of these bands allows to identify the crystallisation points where the glass is structurally weaker and, therefore, could be more subject to breakage when exposed to external stress. The model can be extended and generalised for any other glass formulation. In this way it is possible to produce glass with better mechanical characteristics, which respond to different needs depending on their use. In addition to this promising theoretical model, currently, the main practical techniques for strengthening glass involve the use of thermal treatments or chemical tempering of the material [11–13].

2.1. Thermal Strengthening

Annealed, heat strengthened and chemically strengthened (or tempered) glass are the three main types of glass for general use. Annealed glass is the "regular" glass, as it comes from industrial glass manufacturing (float glass). Thermal strengthening involves a rapid cooling in air of the annealed glass surface after it has been heated to a temperature above the glass transition temperature T_g and close to the melting point of the material. At the beginning of this cooling process the glass surface cools down and contracts quickly, while its internal core remains hot in order to compensate dimensional changes with small relaxation stress. In this condition, the inner region of the glass is subject to compression while the external one is in tension. When the glass interior cools and contracts, the surfaces are already rigid and therefore residual tensile stresses are created inside the glass while compressive stresses occur at the surface. In comparison to a simple annealed glass, this thermal tempering process increases the strength of the pristine material because the applied stresses must overcome the residual compressive ones on the surface, thus preventing the breaking event [13,113,114]. This allows to increase the mechanical strength of the glass by about 4–5 times (up to a few hundred of MPa) and, at the same time, guarantees a better behaviour of the material in terms of safety when it is subject to a breakage [115]. In fact, when this event occurs, this kind of glass generally shatters into many small non-sharp and quite harmless fragments unlike what happens for annealed glasses which break in larger pieces, with a dangerous dagger-like profile. This particular response of tempered glass to a breakage event can be explained by the high strain energy present within these materials. The main limitation of the thermal strengthening process is linked to the minimum thickness obtainable for a tempered glass, which cannot reach values lower than a few millimetres (around 2–3 mm, typically) due to the rapid cooling process and the substantial difference in cooling rate from the glass core to its surface. This inevitably imposes further limits on the geometry and shape of the final products made with this type of glass, which must be simple and not very elaborate [11–13,67]. For all these reasons, thermally tempered glass finds its widest use in all those applications where human safety becomes an issue, such as in the automotive sector, for the development of side and rear windows in the vehicles, in the architectural one for the realisation of safety glass doors in private and public buildings, in the domestic environment (see, for instance, the glass for showers or microwave ovens), and the military/civil sector for the development of bulletproof glass where tempered glass is an essential component.

2.2. Chemical Strengthening

Another method to increase the strength of a multicomponent oxide glass involves modifying its chemical composition, replacing one of its constituent elements with another one that is different in terms of atomic dimensions and electronic polarizability and, at the same time, without significantly changing the network structure of the pristine glass. In particular, the replacement of small ions (originally present in the glass matrix) by larger ones (coming from an external ion source) produces a compressive stress at the surface of the glass for a "stuffing" or "crowding" effect, which can improve the glass strength by counteracting the surface flaws. This compressive stress at the surface is compensated by a tensile one in the internal region of the glass [7,11–13,110]. Generally, this method is applied at a temperature lower than the glass transition temperature T_g and involves the use of a mixture of molten salts as an ion source. For this reason, the "chemical strengthening" method is also referred to as "ion-exchange strengthening". This technique prevents any risk of surface deformation and geometrical distortion due to the temperature parameter if compared to the thermal strengthening method. The resulting compressive stress so generated is generally higher than that achievable with the thermal tempering approach and it is confined in a thinner region of the glass, immediately below its surface, for low process temperature. In this case, the maximum compressive stress obtainable with this technique ranges from several hundreds of MPa to around 1 GPa in proximity of the glass surface [110,116]. Conversely, for a high process temperature (i.e.,

close to the glass T_g or above), the position of this maximum is located several microns below the glass surface and the magnitude of the stress rate decreases for the occurrence of surface stress relaxation due to viscous flow of the glass [13]. On the other hand, for a same process temperature, the maximum of the surface compressive stress decreases when the ion-exchange time increases: the depth at which the residual stress equals zero (i.e., the depth of layer, DoL) becomes deeper and, consequently, the flaws that can be involved in the process are larger [110,117,118]. On the other hand, the maximum for the tensile stress is not so easy to identify but, in some cases, it is located immediately below the compressive zone and its value is an order of magnitude lower than that of the compressive stress (~few tens of MPa), depending on the process duration and sample thickness [13]. Figure 1 compares the residual stress profile in the case of thermally and chemically toughened glass, respectively. Due to the stuffing effect of the incoming ions at the glass surface, the chemical strengthening method presents both large surface compression and internal tensile stress. The transition from the compression zone to the tension one is quite sharp. Conversely, the residual stress distribution in a thermal tempered glass takes on a parabolic profile depending on the temperature distribution achieved during the cooling step of the thermal tempering process. In this case, the compressive stress at the surface is approximatively twice the value of the tensile stress inside the specimen [11–13].
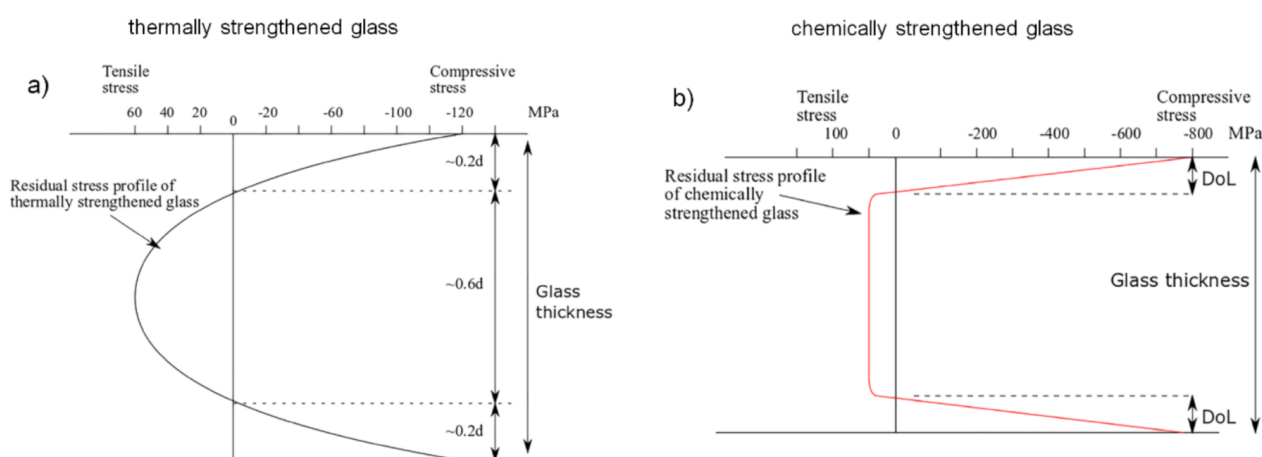

Figure 1. Residual stress profile through the glass thickness for: (**a**) thermally tempered glass; (**b**) chemically toughened glass. d is the glass thickness; DoL is the depth of layer. Figure reprinted from [67] under the terms of the Creative Commons Attribution 4.0 International License.

Several approaches have been proposed for stress evaluation in chemically toughened glasses. Generally, they are based on Cooper's method which provides the determination of the stress in the glass starting from the knowledge of the concentration gradient for the ions participating in the exchange process [7,119]. In this context, R. Dugnani developed an analytical solution to the problem assuming a generalised function for the stress relaxation, a constant ionic inter-diffusion coefficient and, simultaneously, taking into account an analytical approximation for the composition-dependent stress relaxation behaviour of the glass [120]. On the other hand, A. K. Varshneya, G. Macrelli, and others in their studies modified the Cooper's analysis introducing a new term in the model, related to different relaxation contributions (i.e., the viscoelastic and structural one) together with the network hydrostatic yield strength in order to evaluate the subsurface maximum compressive stress when the process temperature is higher and/or close to the glass transition temperature T_g [121–124]. Also noteworthy is the method, recently proposed by R. Rogoziński, which allows to control in real time the stresses generated in a glass as a result of the ion-exchange process from the knowledge of some parameters such as the elasto-optical coefficients, the dependence of the diffusion coefficients on the temperature and, finally, the function describing the time relaxation of stresses at the glass surface [118]. Differently from the

numerical and analytical approaches mentioned above, N. Terakado and co-workers have developed a very original method for evaluating the compressive stress in a chemically strengthened glass, connecting it directly to the glass structure on an atomic scale. The non-contact and non-destructive method is based on the "stuffing" effect and the knowledge of three structural parameters, represented by specific boson peaks in the micro-Raman spectra of the sample [125].

At the end of this brief overview on the main concepts underlying the chemical strengthening of a glass, it should be remembered that in addition to the two most important process parameters, time and temperature, two other factors influence the formation of stress in a chemically strengthened glass: the composition of the pristine glass and that of the molten salt solution in which it is immersed. In fact, the larger the difference between the atomic dimensions of the two ionic species involved in the exchange, the greater is the magnitude of the compressive stress near the surface. In this sense, sodium-potassium ($Na^+ \leftrightarrow K^+$), lithium-sodium ($Li^+ \leftrightarrow Na^+$), or lithium-potassium ($Li^+ \leftrightarrow K^+$) exchanges are able to produce high compressive stresses with values that, practically, are close to 1 GPa in the best cases [11–13]. On the other hand, the composition of the pristine glass plays an important role on the diffusion rate of the ions and stress relaxation of the material during the exchange process. The common soda-lime glass has excellent diffusivity values for the incoming ions but a rapid relaxation process which makes difficult the achievement of a good glass strengthening despite its high alkali content [126]. However, the most promising glass formulation is the one that refers to aluminosilicates which have the highest diffusivity values while ensuring the achievement of compressive stresses well above the possible relaxation effects of the glass matrix [127,128]. In particular, the closer the alumina content is to that of the alkaline oxides, the higher the attainable strength of the glass following the exchange process [129]. For more details on the different characteristics of glass formulations, molten salt compositions, and ion-exchange typologies in glass strengthening, the reader is referred to the exhaustive reviews on the subject [11–13]. The main features of the two glass strengthening processes described above are compared in Table 1 below.

Table 1. A comparison between thermal and chemical glass strengthening methods.

Parameter	Thermal Strengthening	Chemical Strengthening
Strength (max. value range)	~(200–400) MPa	~(800–1000) MPa
Surface compression layer	Thick	Thin
Stress distribution profile	Parabolic	More flat & square
Minimum sample thickness	2–3 mm	<1 mm
Process Time	Short (mins)	Long (hours)
Process Cost	Cheap	Expensive
Glass Composition	No relevant	Alkaline glass (i.e., soda-lime or aluminosilicate)
Product Shape	Simple geometries	Unusual shape

2.3. Chemical Strengthening: Applications

Although the chemical toughening process of glass presents expensive production costs due to its high time consuming if compared with a simple thermal tempering process, the possibility of obtaining greater mechanical strengthening in large glass surfaces with small thicknesses makes this process particularly suitable for many technological applications, ranging from the architectural (e.g., windows for buildings and palaces), automotive and transport sectors (e.g., windshield for airplanes and vehicles) up to the electronics and military ones (e.g., panels for displays in many electronic devices; air-to-ground missile launch tube protective covers). Figure 2 shows some outstanding applications related to chemical strengthened glasses.
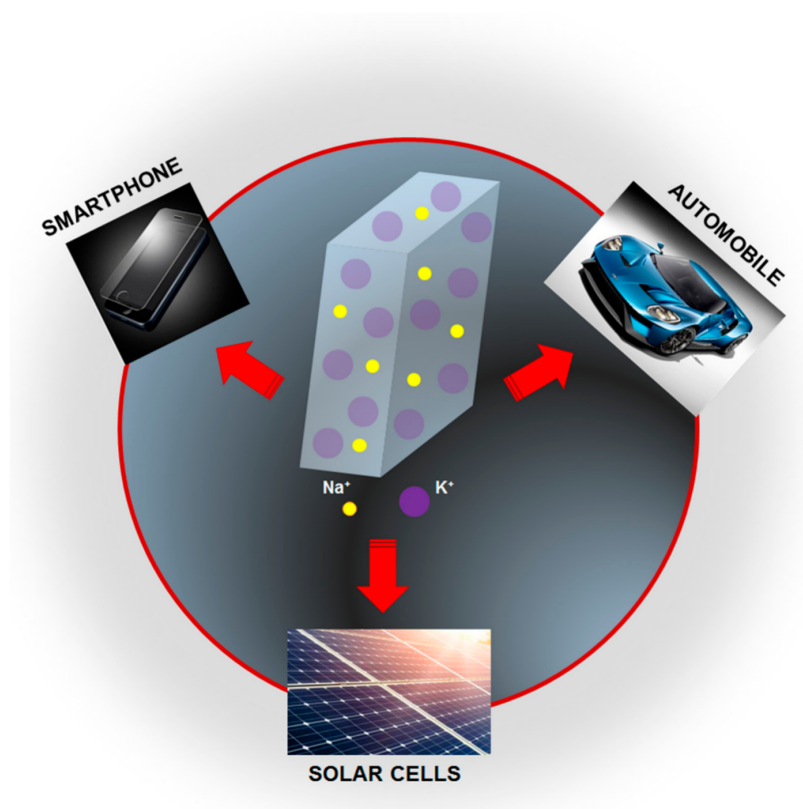
Figure 2. Some relevant application fields of glass chemical strengthening.

In daily life, storing and sharing of data, from those personal to public ones, is almost delegated to electronic devices, such as smartphones, tablets, and lap-tops. The safety of these data does not only concern their protection at software level from any external attacks or a sudden failure of the operating system, but also requires the physical protection of the same devices, with particular reference to some of their most vulnerable elements such as monitor and/or display.

For this reason, CORNING® Inc., Asahi Glass Corporation (AGC), and SCHOTT AG, three world leaders in glass manufacturing, have developed in the recent years different high ion-exchange (HIE) tempered aluminosilicate glasses (for instance, the Gorilla® series from CORNING®, the Dragontrail™ from AGC, and the Xensation series from SCHOTT AG, respectively) with outstanding resistance to breakage and scratches in order to increase the protection for cover and touch screens, greatly reducing the risk of damage due to potential impact or fall and, consequently, avoiding any repair costs associated with this unpleasant event [130–133].

In all these cases, the characteristics of high surface resistance (>900 MPa in the best cases), flexibility (>700 MPa as a bending stress) and lightness (glass thickness < 1 mm, generally) are conferred to the pristine aluminosilicate glasses by the special chemical tempering treatment based on $Na^+ \leftrightarrow K^+$ ion-exchange, where the large K^+ ions, substituting the host Na^+ ions, force the generation of surface compression stress, supporting the closure of the cracks, thereby increasing the strength of the material and preventing the formation of others.

In this context, Apple, although employing Corning Gorilla glass technology to protect the displays of its smart devices, in recent years made a strong effort in the search of alternative solutions to further increase the conventional method of glass strengthening. Different strategies have been investigated, such as the implementation of a patterned asymmetric method based on double ion-exchange process in order to increase the compression depth over at least one localized region, with particular reference to the bend zones of the glass cover, as highlighted in some Apple patents recently published by the US Patent &

Trademark Office [134–136]. Regarding the bulk material, the choice of the manufacturing company fell on a lithium aluminosilicate glass for its excellent chemical durability and mechanical resistance. The whole toughening process consists of two ion-exchange steps. In the first one, the specimen is immersed in a sodium nitrate $NaNO_3$ salt (concentration range: 30–100% mol.) at a temperature lower than the T_g of the glass (process temperature range: 350–450 °C) for 4–5 h. In this case, the sodium ions, originally present in the melted salt, may exchange for smaller lithium ions in the glass matrix. This contributes to a first glass strengthening, allowing a build-up of sodium ions at the specimen surface. The second ion-exchange step, carried out in a potassium nitrate KNO_3 salt (concentration range: 30–100% mol.) at a temperature lower than the glass T_g (process temperature range: 300–500 °C) for a process duration of 6–20 h, contributes to the definitive toughening of the glass. This double ion-exchange process was adopted by Apple both for the realisation of the front and rear glass cover of the iPhone11 smartphone generation. Moreover, the rear glass cover is also loaded with metal elements—through diffusion or deposition processes—in order to guarantee wireless charging operation for the final device.

Corning response to Apple arrived quickly with its Gorilla® Glass Victus™, a chemically treated aluminosilicate glass capable of guarantee the best performance in terms of drop (up to 2 m) and scratch resistance among all the glasses belonging to the Gorilla® family. The Gorilla® Glass Victus™ presents a minimum thickness of about 0.4 mm and a shear modulus equal to 31.4 GPa, fully responding to the need for high mechanical strength in small thicknesses [137]. Due to these remarkable features, this cover glass was adopted by Samsung in some of its products such as, for instance, the Galaxy Note 20 Ultra.

Finally, it should be mentioned that the race for increasingly resistant materials is moving towards the use of glass-ceramics, characterized by the presence of nanocrystals within the amorphous glass matrix. In fact, a glass-ceramic is born like glass and then turns into an almost completely crystalline substrate by an ad-hoc thermal treatment able to induce the nanoparticle formation from additional nucleating agents, such as silver or titanium, previously introduced in the glass matrix. The dimensions of these nanostructures are generally of the order of a few nanometres, thus allowing an excellent transparency of the material. Moreover, glass-ceramics are tough, lightweight and present high temperature stability, high resistivity and excellent isolation capabilities. All these features are well suited to the role that these materials must assume in terms of safety of smart electronic systems. It is therefore no coincidence that, at the release of the new iPhone12 series in October 2020, Apple declared that it had realized—in collaboration with Corning—a new extremely resistant glass-ceramic product, the Ceramic Shield, four times better in terms of drop performance than Gorilla® Glass Victus™ [138]. Although Apple is not the first to have used glass-ceramic materials for the protection of its smart electronic devices (see, for instance, the Samsung with its smartphone Samsung Galaxy S10), the company from Cupertino is however the first to use such materials for the display protection while other manufacturing companies, such as Samsung, have used this material for back panel or camera-lens safety.

The chemical strengthening process of glass has recently found its application also in the automotive sector. In 2017, the American automotive manufacturer Ford was the first to equip its flagship automobile, the Ford GT supercar, using Gorilla glass for the windshield, rear window and engine cover of the vehicle, replacing the use of more traditional tempered glass. The new Gorilla hybrid glass, designed in strict collaboration with Corning, allowed a lightening of the overall weight of the automobile by well over 5 kg, increasing its manoeuvrability and reducing fuel consumption as well as the risk of glass breaking. Instead of using two thermally tempered sheets, joined together by a transparent thermoplastic adhesive in order to form the classic windshield glass, the new solution uses the co-presence of three layers: an external tempered glass joined to an internal one, highly resistant and chemically toughened, by a transparent and sound-absorbing thermoplastic. The presence of the ion-exchanged glass contributed to reduce the overall thickness of the new hybrid glass by approximately 50% compared to a common

windscreen made with thermally tempered glass. Given the advantages of this strategy, it is likely that in the future the same technology will be extended to the production of series cars [139,140].

As a third significant example of ion-exchange application for glass strengthening, the case of photovoltaic and space solar cells deserves consideration. In fact, the cover glass represents one of the fundamental components of each of these devices and plays a key role in the final cost and efficiency of the cells. In terms of cost, the contribution relating to the protective glass is not negligible because it alone represents about 25% of the total cost of the whole device. Moreover, regarding the cell efficiency, the protective glass can influence the device performance depending on the transparency level of its material to solar radiation. Therefore, the optimisation of the cell cover glass becomes extremely important in order to minimize costs and maintain high performance for the final product.

In principle, glasses for photovoltaic and space solar cells should be as lightweight as possible in order to reduce material thickness and waste, so decreasing the overall cost of the device. Usually, commercial, thermally toughened float or soda-lime glasses, with a thickness of around 3 mm, are adopted on-board of the photovoltaic cells while they appear quite bulky and heavy for space solar cells. As a direct consequence of using a thin cover glass, comes the need for greater strength of the material. Moreover, the glass composition should be engineered for low losses and small UV photon absorption in order to guarantee better cell efficiency and service lifetime, respectively [67]. The use of chemically strengthened glasses may represent a valid solution, as reported by H. Wang et al. [141]. In that work, the authors demonstrated how an ion-exchange process, performed in a bath of pure KNO_3 molten salt at a temperature comprised between 400 °C and 460 °C for a process time from 20 to 90 min, was able to confer suitable toughening to experimental silicate glasses having a thickness of only 120 µm. In particular, the maximum achievable flexural strength was measured to be around 632 MPa, four times higher than that of the un-treated samples. Moreover, the selected ionic process did not significantly modify the transparency characteristic of the pristine glasses in a wide range of the wavelength, while, at the same time, it was able to increase the durability of the material when exposed to the ion radiation. Hence, the obtained results were in full agreement with the possibility to reduce the cost and improve the performance of the space solar cell in terms of efficiency and service lifetime.

With the aim to release on the market a lighter glass, the researchers of the Asahi Glass Corporation (AGC) made a novel chemically-strengthened industrial glass, Leoflex™, an ultra-thin, flexible and extremely resistant material. Leoflex™ glass, with its lower sodium concentration at the surface, exhibits better electrical resistivity and higher mechanical strength caused by the chemical toughening process and strongly reduces the risk of potential induced degradation (PID), which represents one of the main reasons for the failure of photovoltaic and space solar cells. All these features made this material an ideal candidate as a cover glass for the development of highly performing photovoltaic application [142]. Additionally, the ion-exchange process also plays a key role in the efficiency of the same cell by introducing noble metal ions/nanoparticles capable of triggering particular energy transfer mechanisms (i.e., down-conversion from ultraviolet (UV) to visible wavelengths or up-conversion from infrared (IR) to visible range), especially when the glasses are doped with elements belonging to the rare earth group. This subject, together with other ones which involve the use of metal aggregates for different application fields, will be addressed in the next section.

3. Noble Metal Ions/Nanoparticles by Ion-Exchange in Glass Substrates: Novel Platform for Photonic & Sensing Applications

3.1. Ion-Exchanged Noble Metal Ions/Nanoparticles in Rare-Earth—Doped Glasses for Enhanced Light Sources and Photovoltaic Cells

The development of solid-state light sources by using glasses doped with different combinations of rare earths has driven the attempts to further improve their efficiency by using sensitisers added to the glass matrix. Their function is to increase the absorption of

the excitation light, also at wavelengths where more efficient, reliable, and less expensive pump sources are available, and efficiently transfer the collected energy to the emitting rare earths.

The same materials can also be tested to be used to enhance the efficiency of photovoltaic (PV) cells.

In fact, a large portion of solar radiation in the UV spectrum cannot be absorbed or efficiently converted in electricity by silicon-based PV systems. In case the solar light in the spectral windows where PV cells are less efficient could be converted entirely inside the working wavelength interval of the cells, their theoretical efficiency would increase from 29% to 38%. It is therefore apparent that even a more realistic partial result could be a crucial improvement.

Many approaches have been pursued, but, as we will describe in the following, usually metallic silver nanoparticles have been used as sensitizer. Their advantage is a strong broadband absorption band, joined to the possibility of introducing them in the glass by means of ion-exchange and subsequent thermal processes, which makes this mature technological approach fairly convenient and economical.

Malta et al. reported, in 1985, the enhancement of Eu^{3+} luminescence in melted calcium boron oxy-fluoride glass, which they related to the local field enhancement produced by the surface plasmon resonance of the Ag particles [54]. In this case, silver was introduced directly in the glass melting process. This result was confirmed by Hayakawa et al. in sol-gel glasses where reduction of the silver ions to metallic form was obtained by annealing the glass in H_2/N_2 atmosphere [55]. Similarly, Li et al. demonstrated for the first time non resonant energy transfer from Ag^+ ions (hence, non-metallic) to Dy^{3+}, Sm^{3+} and Tb^{3+} [143].

These are only few of many examples of rare earth doped glasses where ion-exchange was not used as a means for introducing silver nanoparticles in the glass and that showed the potential of using silver as sensitiser. In the following, we will focus on and limit to examples where ion-exchange was applied.

Jiao et al. investigated the effects of silver introduced by ion-exchange in sodium borate glasses on Eu^{2+} and Eu^{3+} ions fluorescence [144]. The authors stressed the different role that few Ag atom/ion complexes, up to full grown nanoparticles, may play in influencing fluorescence emission. Actually, after introducing silver in the glass, typical emission of both Eu^{2+} and Eu^{3+} ions increased, but excitation would switch from the 270 nm band of Ag^+ ions to the 350 nm ascribed to Ag clusters, which get formed at expense of Ag^+ isolated ions and smaller aggregations by increasing ion-exchange time. Using 350 nm excitation, an otherwise weak band assigned to the $4f^6\,5d \rightarrow 4f^7$ transition of Eu^{2+} ions was also enhanced. Therefore, it is evident how in this case both the optimal excitation and the emission depend on the valence and aggregation of silver, which can be controlled by the ion-exchange process parameters.

Similarly, Li et al. studied the effects of silver doping by ion-exchange on the photoluminescence emission in Eu^{3+} sodium-aluminosilicate glass [60]. As shown in Figure 3, the inclusion of silver aggregates produced a broad emission band in the 400-700 nm interval overlapping the Eu^{2+} 5d-4f emission, and a substantial increase of the 615 nm line of Eu^{3+} when excited at 350 nm as the silver content was increased.

The effect was ascribed by the authors solely to energy transfer from silver ions to Eu^{3+} ions. The combined emission by silver, when suitable ion-exchange parameters were chosen, and Eu^{3+} ions produced white light. Therefore, silver contributed both by enhancing Eu^{3+} emission in the red and by its own emission in the blue-green region. The same group of authors has obtained very similar results with Sm^{3+} and Tb^{3+} in the same glass [59,145] and in borosilicate glass [64].

Strohhöfer and Polman demonstrated energy transfer from silver ions/dymers to erbium ions implanted in BK7 after Ag^+/K^+ ion-exchange [56].
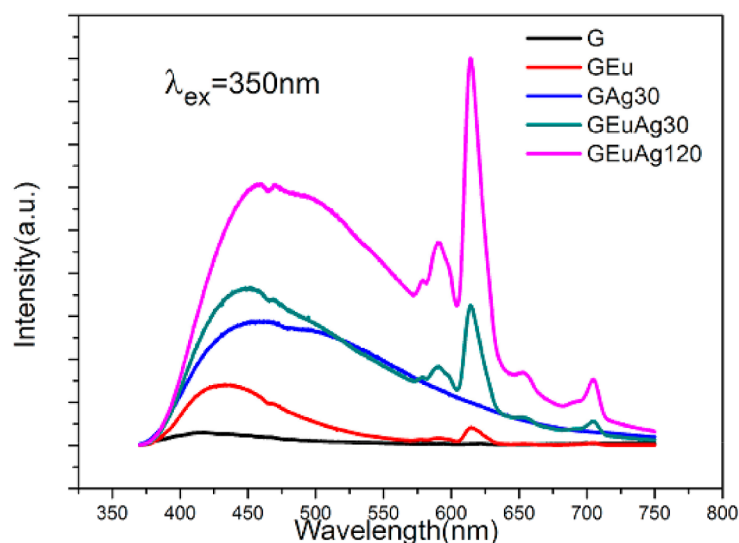
Figure 3. Photoluminescence emission of Eu^{3+} doped sodium-aluminosilicate glass as a function of the silver ions density. Reprinted with permission from [60] © The Optical Society.

Our research group has characterised very thin wafers of Er^{3+}-doped silicate glasses entirely ion-exchanged in an $Ag/NaNO_3$ melt. [57,58]. We tested several post-exchange annealing processes evidencing the effect on absorption and emission spectra. In particular, since Er^{3+} resonant excitation was not affected by the silver presence, whereas non-resonant was enhanced (up to 100 times), we concluded that the effect should be ascribed to energy transfer from the silver nanoparticles to the Er^{3+} ions, rather than local field enhancement.

Similar results have been demonstrated in different Er^{3+}/Yb^{3+} glass formulations, such as silicate and titanoniobophosphate glasses, where planar waveguides have been fabricated by Ag^+/Na^+ ion-exchange [62,146].

Photoluminescence enhancement of Dy^{3+}/Eu^{3+} co-doped tellurite glasses was reported by Yu and co-workers [78]. In this case, the quantum efficiency improvement (several % units, depending on excitation wavelength, ion-exchange conditions and glass doping) was attributed mainly to the local plasmon resonance field enhancement produced by the silver nanoparticles. Also in this case, different ion-exchange parameters produce glasses capable of emitting with different CIE (Commission Internationale de l'Éclairage) coordinates, and therefore emission tailoring is readily possible.

Recently, the Yb^{3+}/Ho^{3+} doping system, interesting for the fabrication of laser sources for medical applications operating at 2 µm, has been studied by Vařák et al. in zinc-silicate glasses [147]. In this case, Ag^+/Na^+ and Cu^{2+}/Na^+ ion-exchanges have been tested, in order to introduce either silver or copper nanoparticles inside the glass. In both cases, planar waveguides were obtained and characterised. Regarding photoluminescence, unfortunately the effect of copper was, even if only slightly, negative, since the emission decreased after ion-exchange, and a subsequent annealing step did not improve it. The effect of silver was however better, and a 20% photoluminescence intensity increase, assigned to energy transfer from silver clusters to Ho^{3+} ions, was measured.

Silver ion-exchange has been reported to enhance NIR emission also when not using rare earths, as with Bi-doped silicogermanate glasses [148]. In fact, lower valence Bi ions are responsible for NIR fluorescence, so that increasing their presence can improve the low efficiency of fibre amplifiers based on this element. In this case, the effect of silver ions introduced in the glass by ion-exchange followed by thermal annealing is not linked to energy transfer processes, but rather to the valence reduction effect on the Bi^{3+} ions. This can be efficiently achieved only by introducing silver ions by ion-exchange, since the required valence state of silver is given by the process itself. The authors showed that Bi emission in the visible range was reduced and NIR emission increased by about twofold this process.

However, the presence of silver does not always enhance photoluminescence emission. In fact, as described for Ce-doped soda-lime silicate glasses by Paje et al. [149], silver causes the reaction:

$$Ce^{3+} + Ag^+ \rightarrow Ce^{4+} + Ag^0.$$
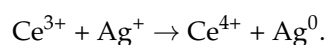
This in turn not only changes the emission photoluminescence spectrum but also its intensity, since Ce^{4+} ions do not emit and even absorb both the UV excitation and the photoluminescence produced by Ce^{3+} ions.

In the case of photo-thermo-refractive (PTR) glasses, however, the same type of reaction has been exploited by Sgybnev et al. [74] to test the potential of these sodium-zinc-aluminosilicate glasses co-doped with Ce and Sb to serve as wavelength converters for enhancing the efficiency of PV cells. The authors tested the possibility of producing neutral silver molecular clusters in PTR glasses both by irradiating with UV radiation samples already doped with silver in bulk or by Ag^+/Na^+ ion-exchange. In both cases an annealing step followed the first phase of the process.

As a result, in all cases, silver molecular crystals were obtained, but their efficiency was different depending on the process. The PV cells placed behind the best sample obtained by ion-exchange reduced their overall efficiency, even if only slightly, whereas the sample with silver atoms dispersed at the time of initial melting showed a slight efficiency improvement respect to the as-synthesised cover glass.

3.2. Ion-Exchanged Noble Metal Nanoparticles in Glasses for Sers Applications

The interaction between light and noble metal nanoparticles (NP) at the material interface is the key point for the employment of one of the best performing optical investigation methods: the surface-enhanced Raman scattering (SERS) technique. These metallic nanostructures work as "hot spots" for the electric field of an interacting lightwave by means of the localised surface plasmon resonance (LSPR) effect [150]. When a molecule is close to one of these "hot spot", its Raman signal increases by several order of magnitude under the action of the enhanced field. This confers to the sensors/biosensors based on this optical technique ultra-sensitive detection limits, combined with the structural information content typical of the Raman spectroscopy [151].

For the development of high-performance SERS devices, the optimisation of the substrates is mandatory. Ideal SERS platforms should ensure high efficiency (in terms of signal enhancement), reproducibility in response, reusability, long-term stability for the metal nanoparticles, low cost, and simplicity of the fabrication method [97,152]. Furthermore, considering that silver NPs—which offer the best SERS activity among all noble metal nanostructures—are prone to oxidation and sulfidation phenomena, it is easy to understand how obtaining SERS substrates adhering to ideal requirements is still a challenging task.

Among all the materials and manufacturing methods for SERS substrates [153], ion-exchange in glass may represent an effective route towards the realisation of performing and reliable SERS platforms thanks to the following features: (i) efficient SERS activity of these substrates (from 10^5 to 10^7 signal enhancement); (ii) intrinsically low material and processing costs; (iii) adequate sample reproducibility by opportunely tailoring the process and post-process parameters; (iv) long-term stability for the metal nanoparticles by their embedding within the glass matrix (typically, tens/hundreds nanometres under the glass surface) during a suitable post-process treatment; (v) actual sample reusability by partial exposure of noble metal nanostructures at the surface and their further refresh through suitable chemical and/or thermal steps [105,154].

3.2.1. Glasses for SERS Substrate by Ion-Exchange Technique

Soda-lime and float glasses with their large commercial availability, high transparency, good chemical durability, high sodium content, and ion inter-diffusion coefficients are the most popular material for the realisation of SERS substrates by ion-exchange process. The presence in trace of some impurities, such as iron or arsenic, within these glasses

promotes the reduction of the exchanged noble metal ions into metallic clusters during the subsequent sample treatment [100,155–158].

Not to be forgotten are the commercial borosilicate glasses (e.g., Schott BK7 or Corning 0211 glasses) which, with their higher purity, are the most common substrates for the realisation of integrated optical devices by ion-exchange process. Although the almost total absence of impurities does not make them suitable for the formation of metal nanoparticles by chemical reduction processes, recent studies have shown the possibility of obtaining efficient SERS substrates also by using these highly pure glasses [159].

Finally, it should also be mentioned that, together with these widely used glass systems, phosphate or fluorophosphate glasses are recently gaining ever-increasing interest due to their lower processing temperature, higher diffusion coefficient for noble metal ions, and better reducing properties thanks to the large concentration of non-bridging oxygens generated during the glass synthesis [99,160].

Having incorporated the metal ions in the glass matrix by the ion-exchange process, one can promote their precipitation into metal nanoparticles by adopting different strategies, as described below.

3.2.2. Thermal Annealing in Air (O$_2$ Atmosphere)

The most common and simple strategy is represented by a thermal annealing treatment, carried out in air (O$_2$) in a suitable furnace, at a temperature close to the transition temperature T$_g$ of the glass. The mechanism that regulates the formation of silver NPs inside an ion-exchanged soda-lime glass by means of this thermal post-process is well explained in the work of A. Simo et al. and outlined in Figure 4 below [106].
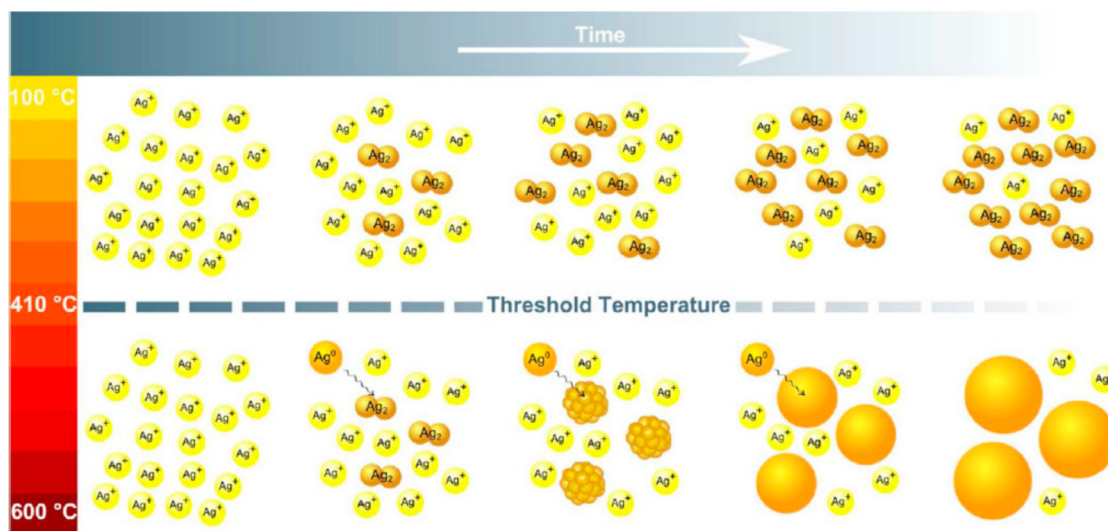

Figure 4. Outline of the mechanism regulating the formation of silver clusters and particle growth in soda-lime ion-exchanged glass under thermal annealing in air at different time and temperature. Reprinted with permission from [106]. Copyright © 2012, American Chemical Society.

After the ion-exchange process, only Ag+ ions are present within the glass. By increasing the annealing time and temperature (providing that the temperature remains below the critical threshold of about 400 °C), there is an increasingly large formation of silver clusters, which occur in the status of dimers Ag$_2$ (diameter size d < 1 nm). These small clusters are stable at elevated temperatures and remain within the glass matrix. The presence of these non-plasmonic nanostructures is the first responsible for the photoluminescence enhancement of the ion-exchanged sample. Thermal treatment performed beyond the aforementioned threshold temperature, which corresponds to the decomposition temperature of silver oxide, leads to the formation and the further growth of metallic silver NPs as the exchange time increases and the process temperature approaches Tg. In fact, in this

temperature range, the number of reducing agents—the non-bridging oxygens (NBOs)—increases inside the glass matrix while the number of silver clusters remains unchanged. Consequently, the existing clusters begin to grow through the progressive addition of silver atoms Ag0 (monomers) towards the formation of ever larger plasmonic metal NPs, while the overall concentration of the particles remains constant.

Therefore, for a given temperature, the final size of these metal nanostructures is determined by the concentration of the dimers Ag_2 and the duration of the heat treatment. Typically, the formation of these particles is limited to the layers immediately below the glass surface, at a depth of a few tens/hundreds of nanometres, due to temperature-induced diffusion effects. Differently from the silver cluster case, the presence of these plasmonic metal nanoparticles produces a quenching effect on the photoluminescence intensity of the ion-exchanged specimen, especially when their size reaches several tens of nanometres or, at most, a few hundred nanometres [106].

3.2.3. Thermal Annealing in H_2 Controlled Atmosphere

Another thermal post-processing strategy for a glass exchanged with noble metal ions involves the heating of the sample in a controlled hydrogen (H_2) atmosphere. Although this technique requires larger precautions for the operator safety in comparison with that performed in air (O_2), this thermal post-process favours the formation of both glass-metal nanocomposite (GMN) species within the glass and metal island film (MIF) on the glass surface due to the out-diffusion mechanism of the noble metal atoms as a result of the hydrogen penetration into the glass [161]. However, under particular conditions relating to hydrogen processing, it is possible to favour the formation of MIF species on the glass surface by minimizing that of GMN within the host material, as well reported in the works of A. Lipovskii and collaborators, to which we refer for more details [162–164]. In brief, the authors employed a thermal poling technique, through the use of a suitably shaped anodic electrode applied to the ion-exchanged silicate glass sample, in order to modify the distribution of noble metal ions (e.g., Ag^+) and thus control the formation of the metal nanoislands by means of a soft thermal annealing step in a hydrogen atmosphere. Figure 5 explains this approach together with an atomic force microscopy (AFM) image of the nanoislands so formed. Depending on the electrode periodicity, arrays of nanoislands can be obtained on the surface of the glass sample.
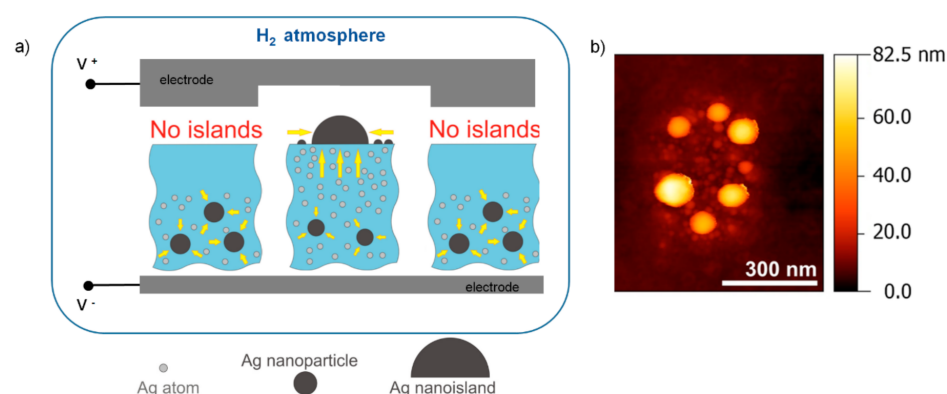

Figure 5. (**a**) A sketch of the mechanism of silver nanoislands growth by poling treatment following by a thermal annealing treatment in H_2 controlled atmosphere; (**b**) an AFM image of a nanoisland group in a not poled region after annealing treatment in H_2. Figure adapted from paper [164] under the terms of the Creative Commons Attribution 4.0 International License.

During the poling step, the simultaneous presence of electrostatic repulsion effects generated by the applied DC electric field and those linked to the process temperature favours the migration of the silver ions towards deeper layers of the glass in correspondence of the poled region. Nevertheless, the low poling temperature (T_p ~250 °C) and the lack of impurities in the pristine silicate glass do not favour the formation of silver atoms and

metal nanoparticles in this area. Therefore, if the process parameters (i.e., duration and temperature) of the following thermal annealing in hydrogen are selected in such a way that the hydrogen penetration depth is not enough to reach the diffused silver ions, then any possibility of their reduction is precluded, and the poled zone remains almost empty of silver atoms and nanoparticles. On the contrary, in correspondence with the non-poled zone, the hydrogen in-diffusion is accompanied by an out-diffusion of the silver ions with their consequent reduction and formation of metal nanoislands on the glass surface [163]. A similar result was found by E. Kolobkva et al. in fluorophosphate glasses [99]. The possibility of drawing 2D-patterned nanoisland structures on the glass surface makes these substrates ready for their use in SERS applications.

3.2.4. Laser Irradiation Techniques

Besides the aforementioned thermal post-processes, other annealing techniques involve the use of continuous [102,165–167] and/or pulsed lasers [98,101,168–171] working at different wavelengths of the spectrum (from X-ray to ultraviolet (UV) and visible (VIS) regions up to infrared (IR) ones) and able to effectively reduce the noble metal ions in metal NPs. In this case, the mechanism of nanoparticle formation depends on the power of the laser source at the surface of the ion-exchanged specimen. In fact, in many cases the interaction between the laser beam and the sample is of thermal nature, as occurs for silver-ion-doped glasses when the working wavelength of the light source falls in the sample absorption region (i.e., from the UV to visible band, depending on the electronic status of silver). If the power level of the laser is relatively low, so as to ensure that the temperature of the irradiated area remains close to the glass transition temperature T_g during the whole process, then the reduction in silver atoms follows a trend almost similar to that of the thermal annealing mentioned above (in O_2 environment): laser irradiation produces free electrons from the non-bridging oxygens (NBOs) which are captured by the Ag^+ ions to form neutral Ag^0 atoms (metal silver atoms), starting their following growth process in metal NPs. As in the previous case, the nanoparticles thus formed are completely embedded within the glass matrix and a further etching step is required to make them partially exposed on the surface. This makes them available for SERS applications.

Conversely, at higher laser power levels, the temperature of the glass surface becomes greater than the glass T_g and the sample, in the irradiated region, behaves as a molten glass. In this liquid state, some of the silver nanoparticles are formed in a deeper region of the irradiated area while others may migrate to the glass surface where they are constrained to remain under the effect of the surface tension. Here, following the temperature distribution, they move towards the edges of the laser beam where they continue to aggregate forming larger structures. Once the laser is turned off, these nanoparticles remain frozen and partially exposed to the air [102,165,167]. In this way, these metal nanostructures are ready for SERS sensing and no further etching step is required. If compared with the standard thermal annealing process in air, the one induced by laser irradiation is faster in terms of nanoparticle formation and offers the non-negligible advantage of being able to draw ordered structures of nanoparticles—equally spaced from each other—so that the SERS response of the substrate is enhanced [102,166]. Figure 6 sketches the mechanism of metal nanostructure formation by high power laser beam in the case of silver ion-exchanged glass (Figure 6a). Figure 6b reports a SEM image of the edge region between irradiated and not-irradiated area. The lack of visible nanostructures on the surface of the exposed region suggests the possibility to obtain silver nanoparticles buried beneath the glass surface. Conversely, densely packed spherical silver NPs, whose size distribution ranges from a few to several tens of nanometres, are clearly visible on the ion-exchanged glass surface at the border of the irradiated area. Figure 6c shows a SEM image of a quasi-periodic arrangement of silver NPs obtained with this technique. Finally, Figure 6d represents a zoom image of an array of silver nanoparticles. The alignment of the nanostructures appears quite regular.
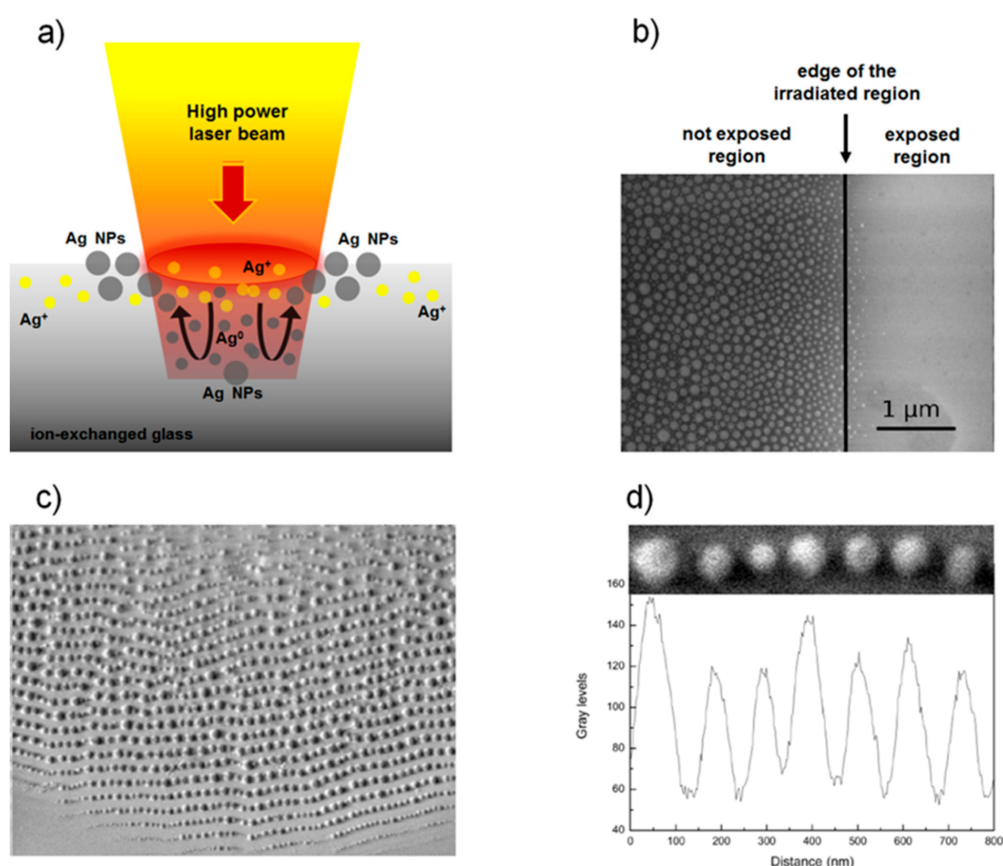
Figure 6. (**a**) Growth process of metal silver nanoparticles on the ion-exchanged sample surface at the edge of an exposed zone by high power laser irradiation; (**b**) a comparison between the distribution of silver nanoparticles in the exposed and not-exposed region, respectively (adapted with permission from [165] © The Optical Society); (**c**) a SEM image of a quasi-periodic arrangement between silver NPs; (**d**) an ordered silver nanoparticle array, with its surface profile plot, obtained by laser beam irradiation technique (reprinted with permission from [166] © The Optical Society).

Obviously, once exposed, these silver NPs can undergo oxidation effects that affect their performance in terms of SERS response. A possible solution to the problem could be to carry out a low temperature thermal annealing in air ($T_{ann} \sim 200\,^{\circ}$ C) in order to reduce to metallic state the thin layer of silver oxide (Ag_2O) thus formed on the nanoparticles surface, which is mainly responsible for the deterioration of the SERS enhancement [102]. Another approach to prevent the aging of silver nanoparticles concerns the deposition of a thin film of transparent dielectric material (e.g., SiO_2, TiO_2, Si_3N_4, Al_2O_3, etc.), provided that the thickness of the deposited layer is such as not to excessively weaken the plasmon resonance and the consequent field enhancement effect. For this purpose, tight thickness control deposition techniques, such as atomic layer deposition (ALD) and plasma-enhanced chemical vapour deposition (PECVD), are preferable [172,173].

3.2.5. Metal Thin Film Deposition for Noble Metal Ions Reduction in Ion Exchange Process

The possibility of realizing SERS active metal nanostructures on high quality, free from impurities, commercial glasses (such as, Corning 0211 borosilicate glass) by means of ion-exchange process can be favoured by applying on the sample surface a metal thin film working as a mask or electrode. In both cases, the presence of the film plays the role of reducing element for the silver ions introduced into the glass following the ion-exchange, as well investigated in the works of Y. Chen and co-workers [103,104,159].

In the masked ion-exchange process in silver molten salts, the reduction mechanism of silver ions in metallic form is strictly related to the presence of electrical potential

differences among the molten salt, the glass and the metal mask. This produces an ionic current flow: the silver ions migrate from the molten salt into the glass through the mask openings, concentrating in the region under the mask edges. Here, by capturing an electron made available by the metal mask, the silver ions are progressively reduced to metallic state [103,104]. Figure 7 shows the effect of a metal mask on the reduction of silver ions following the ion-exchange process.
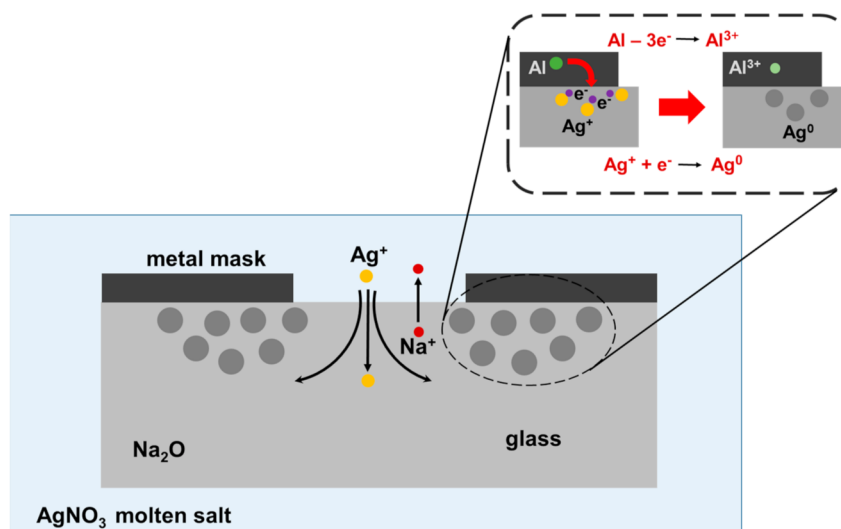

Figure 7. Deposition of silver nanoparticles under the mask edge by masked ion-exchange process (cross-sectional view). In inset, the reduction mechanism of silver ions in metal nanoparticles under an aluminium mask.

The main advantage of this photolithographic approach is to provide the formation of well-defined patterns of silver nanoparticles, aligned with ion-exchange channel waveguides, without any thermal post-processing of the sample. Furthermore, this method represents a valid alternative to that of laser irradiation to realize integrated sensors, based on optical waveguides and SERS.

In the second approach, the deposed metal thin film works as an electrode in a double ion-exchange process. The glass sample is loaded with silver ions through a simple ion-exchange in molten salt. Subsequently, a thin metal film of aluminium is deposited on one of the two sample faces. The sample is then immersed in a potassium molten salt bath. In this way, the overall system represented by the metal thin film, the ion-exchanged glass and the molten salt acts as a real galvanic cell. In fact, two electric potentials are soon established on the two faces of the glass. The first, positive type, is located near the glass-salt interface and takes place from the different inter-diffusivity of the ionic species involved in the process. In this region, the Ag^+ and Na^+ ions diffuse faster in the molten salt than the K^+ ions in the glass. The second, negative type, is generated near the other thin film-molten-salt interface. Here the thin aluminium film tends to release electrons to the Ag^+ ions in the glass while Al^{3+} ions migrate to the molten potassium salt. This electrical potential difference produces an ionic current inside the glass which forces the silver ions to move to the surface of the specimen, in an area immediately below the metal electrode. In this region, the silver ions are reduced in metallic form through the acquisition of an electron coming from the metallic film. The formation of silver nanoparticles is also promoted by the continuous flow of silver ions coming from the deeper regions of the glass towards the interface with the aluminium thin film [159]. Figure 8 describes the mechanism mentioned above (Figure 8a), reporting a scanning electron microscope (SEM) cross-section image of the silver nanoparticles distribution under the sample surface (Figure 8b).
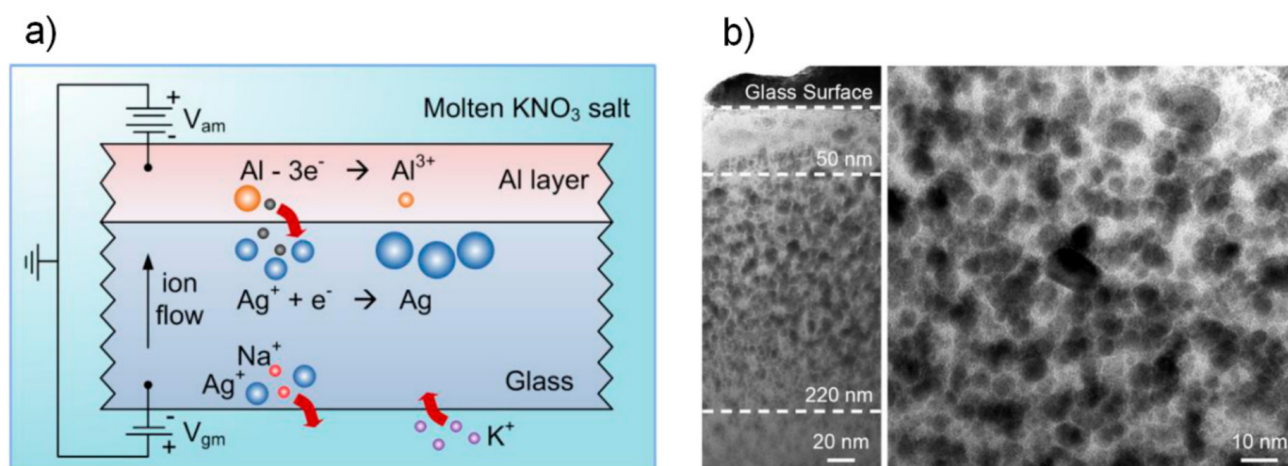
Figure 8. (**a**) Mechanism for the formation of silver nanoparticles in a double ion-exchange using an aluminium thin film as electrode; (**b**) distribution of silver nanoparticles, under the sample surface, following the process (SEM image of the sample cross section near to the surface). Reprinted with permission from [159] © The Optical Society.

The main feature of this method is to offer a simple and low-cost solution for the production of homogeneous and large-scale SERS substrates.

In both approaches described above, the formed silver nanoparticles are embedded within the glass. Therefore, a subsequent soft etching step in HF acid is necessary to expose them at the surface level and make these substrates functional for SERS applications.

We would also like to mention the work of P.L. Inacio et al. for its simplicity. Their investigation, using optical and AFM (atomic force microscopy) measurements, showed a migration of silver Ag^+ cations from inside of the waveguide to its surface at room temperature. Once exposed to air at room temperature, the cations undergo an oxidation process changing the SERS response of the substrate [174]. The advantage of this approach is that it does not require any additional process other than that represented by the aging over time of the exchanged sample. On the other hand, the main drawbacks lie in the rather long aging times, the instability of the SERS substrate over time, and the poor adhesion of the metal nanoparticles formed on the glass surface, which makes them easily removable under the minimum mechanical action or event.

SERS platforms created by ion-exchange are still in their early state, since the main scientific contributions reported so far in the literature demonstrate only proof of concepts of their operation through the use of aromatic molecules (e.g., rhodamine, etc.). However, thanks to their interesting performances both in terms of signal enhancement and detection limit [154], it is likely that soon these substrates will actually be used for the detection of biological targets, such as DNA sequences, proteins, bacteria, etc., as is happening for SERS substrates obtained with different technological approaches [97,151].

4. Perspectives & Future Insights

The high versatility of the ion-exchange process in glass finds new and fascinating perspectives of application in the field of photonics, some of them in progress while others still deserve to be investigated.

4.1. All-Glass Flexible Photonics

As happened for electronics, flexibility is also becoming a fundamental paradigm in photonics, favouring the integration of the respective devices in flexible and stretchable substrates and contributing to expand their application scope, from the field of optical interconnections to that of new systems for the continuous monitoring of patient health, or that of implantable devices for minimally invasive medicine, up to the development of a new class of optical sensors and sources [175–179].

Polymers are certainly the main substrates for the development of this novel technology thanks to their intrinsic mechanical flexibility. In order to give some examples, it is worth listing the possibility of making silicon photonic devices on plastic substrates by means of low temperature approaches (e.g., transfer-and-bond technique, direct fabrication process flow) [180,181]; the deposition of glass-based 1D photonic crystals and erbium activated planar waveguides by radio frequency (RF) sputtering on flexible polymeric substrates [182]; the realisation of stretchable platforms in which single-mode photonic devices, made from high-index chalcogenide glasses and low-index epoxy polymers, are monolithically integrated on polydimethylsiloxane (PDMS) elastomer substrate. In the latter case, local substrate stiffening and spiral based waveguides provide protection to functional photonic components and interconnections with very low radiative optical losses, respectively [183,184]. Polymeric materials, however, exhibit various drawbacks such as a limited range of refractive indices, not negligible optical absorption in the near-infrared region, low process temperature and poor chemical stability. All these factors generally represent serious side effects against their integration and processing with other materials.

Conversely, glass, with a wide range of refractive indices, high transparency from visible to infrared, excellent chemical and thermal stability, as well as low permeation rates for ambient gases and water, may represent a valid alternative as flexible platforms for the realisation of photonic devices provided that their brittleness is somehow mitigated [185]. In this context, J. Lapointe et al. demonstrated the possibility to obtain single mode, low-loss (<0.15 dB/cm), laser-written channel waveguides in flexible chalcogenide glass tape [186]. Nevertheless, among all the glass formulations that can be used for the purpose of flexible photonics, borosilicate glass represents the most widely used material due to its intrinsic characteristics of mechanical strength. In particular, alkali-free commercial borosilicate glasses with extremely thin thicknesses (<100 μm) are currently made available by major glass producers in the format of sheets or rolls. This is the case of Willow® glass from Corning and AF32® from Schott just to mention a few [187,188]. The flexibility of these glasses is conferred through particular manufacturing processes—such as down-draw or roll-to-roll (R2R) techniques—capable of guaranteeing ultra-thin thicknesses to the finished product with an extremely high surface quality, similar to that of a pristine glass [189,190].

As a white sheet of paper waiting to receive the characters from the pen of an inspired writer, so Willow glass with different thickness can be used as a substrate for the realisation of photonic circuits as demonstrated by S. Huang and co-workers. In this case, the writing instrument is represented by a femtosecond laser capable of locally modifying, in the irradiated area, the refractive index of the pristine glass [191]. Figure 9 shows photos of bent waveguides fabricated in Willow glass with different thickness. The scattered green light, coming from a laser source working at 532 nm and injected inside the guiding structures by a butt-coupled optical fibre, visually highlights the actual presence of these channel waveguides.

By optimising the laser processing parameters in terms of speed and energy pulse, it is possible to obtain single-mode channel waveguides at the working wavelength of 1550 nm with propagation loss as low as 0.11 dB/cm in all flexible Willow glass formulations. In particular, for the selected refractive index change ($\Delta n \sim 5 \times 10^{-3}$), the bending losses of the waveguides are practically negligible for a curvature radius $\geq$1.5 cm. Furthermore, the high thermal stability of these optical devices (up to 400 °C), together with the possibility of writing Bragg grating waveguides, opens up new potential scenarios for the realisation of more complex photonic circuits on these commercial flexible glasses. Due to their alkaline-free content, these glasses find one of their main uses in the development of flat panel displays for high-tech applications [192].
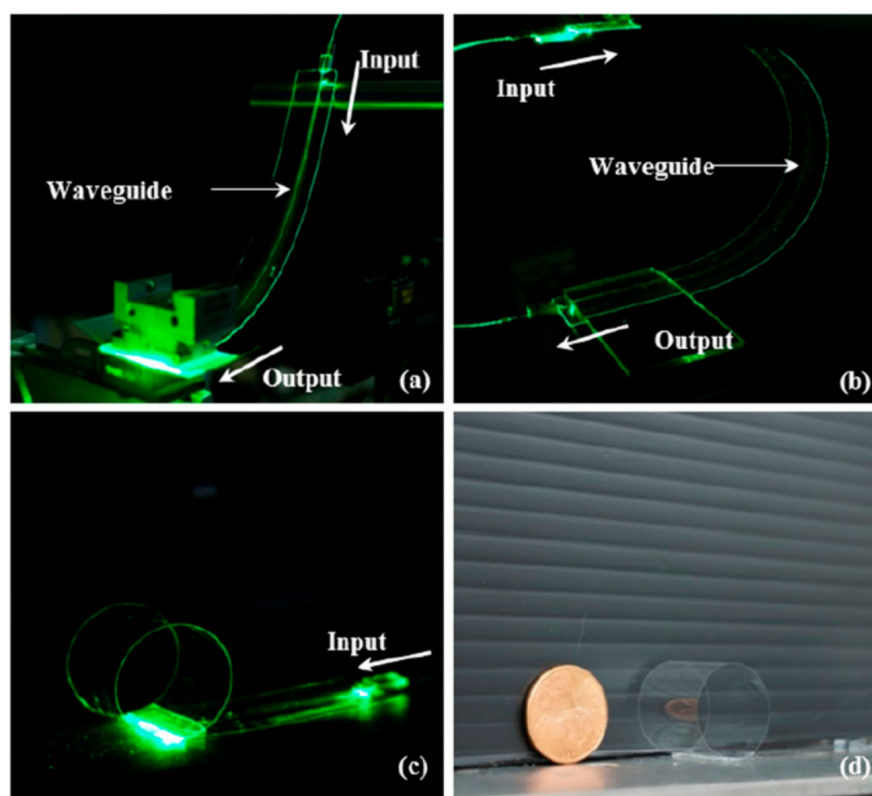
Figure 9. Photos of bent waveguides written by femtosecond laser in Willow glass strips with different thickness and bending radius (**a**) 100 μm thickness and bending radius 13.5 cm; (**b**) 50 μm thickness and bending radius 2.1 cm; (**c**) 25 μm thickness and bending radius 1.0 cm; (**d**) the same sample reported in (**c**) compared with the size of a small coin. Reprinted with permission from [191] © The Optical Society.

The possibility of further strengthening these ultra-thin glasses could prevent the formation of any surface flaws making the customary handling and processing (e.g., glass cleaning, cutting, and lamination) procedures of these products less critical. Nevertheless, thermal tempering does not represent a suitable solution for strengthening these display glasses due to their thinness and low thermal expansion coefficient. On the other hand, the total absence of alkaline ions (e.g., sodium ions, Na^+) in these products would seem to preclude the use of any chemical treatment aimed at further strengthening them. In this context, the interesting work by Mauro et al. would seem to offer an elegant solution to the problem, bypassing this impasse through the use of a particular ion-exchange process in alkali-free boroaluminosilicate glass [193]. The idea behind this original method is to replace ions such as Ca^{2+} and B^{3+} present inside the pristine glass matrix with Ba^{2+} ions coming from an ion source where the sample is immersed. Unfortunately, the kinetics of this kind of ion-exchange would be decidedly limited due to the considerable difference in inter-diffusivity between the two ionic species involved in the process, the alkaline and alkali ones, respectively. Moreover, these alkaline salts present high melting point and chemical corrosiveness that could irreversibly damage the glass surface during the exchange process, making their use as ion sources in a standard ion-exchange practically unfeasible. For all these reasons, the new chemical strengthening treatment is carried out in aqueous solutions of alkaline salts at a relative low temperature and under pressure in order to keep the water stable in its liquid state [194]. Proceeding in this way, the authors demonstrated the possibility to reach surface compressive stresses (CS) of the order of 200 MPa and a depth of layer (DoL) of only a few microns (i.e.,: <2 μm for barium nitrate). This technique can be applied to a wide range of alkali-free glasses, such as ultra-thin

Willow glass, contributing to improve mechanical performance and thus helping to make all-glass flexible photonics more feasible.

A second promising approach towards the development of all-glass flexible photonics is the one that involves the use of alkali-based glass formulations (i.e., sodium aluminosilicate glass). In fact, recent analytical studies conducted by G. Macrelli and co-workers shed new light on the effects induced by the bending stresses on both the mechanical strength and optical properties (e.g., in terms of refractive index) in the two main silicate glass formulations considered here, the alkali-free and the alkali-based ones [195,196]. In general, the thinner the glass, the lower the surface stress resulting from a bending action. This allows to reach ever smaller bending radii, within the limits given by the mechanical strength of the material related to the presence of surface flaws. When subjected to extreme curvature, the glass develops high tension stresses that can lead either to its immediate breakage or to the progressive growth over time of micro-cracks, generated both by the effect of the continuous applied tension and by the action of water vapour on surface flaws, resulting in consequent definitive damage of the material. To overcome this problem, the strategy based on alkali-free glasses dictates a complete sealing of their surface, to make it resistant to the deteriorating action of water vapours on any surface flaws. On the other hand, the strategy based on alkali-silicate glasses involves the use of ion-exchange, capable of strengthening the glass by means of a residual tension profile induced on the surface of the sample following the same process. This suggests that the achievement of the surface flaws stability in extreme bending conditions for the glass represents a key factor to be considered.

From the mechanical analysis carried out on the two types of samples mentioned above it emerges that, under the same extreme bending conditions, the alkali-based silicate glasses strengthened by ion-exchange generally allow larger thickness, overcoming the limitations imposed on not chemically treated alkali-free or alkali-based glasses. Moreover, from an optical point of view, the response of the two types of glass formulation under the same bending stress appears very different in terms of refractive index. In particular, for glasses strengthened by ion-exchange, the presence of residual surface tensions is associated to a local volume change of the material. This induces a further birefringence phenomenon that well overcomes that coming from the bending action of the glass sample. As a result, a strong refractive index gradient occurs at the surface of these exchanged ultra-thin glasses. This effect must be taken into account when designing all-glass photonic devices on this kind of flexible substrates.

From what has been reported up to now it is clear the key role that ion-exchange, together with the glass material engineering, can play in the creation of increasingly performing flexible substrates towards the achievement of an all-glass flexible photonics as valid alternative to that developed on polymeric materials [178].

4.2. New Insight towards the Development of Optical Devices Loaded with Noble Metal Ions/Nanoparticles by Ion-Exchange

Another intriguing prospect of the ion-exchange process that deserves further investigation in the near future is linked to the possibility of realizing new low-cost photonic systems with potentially improved characteristics for a wide application range.

Let consider, for instance, the case of whispering gallery mode (WGM) optical microcavities, which continue to gain a growing interest in the field of photonics for their unique and extraordinary properties. In these microstructures, the light, suitably injected into the cavity, propagates grazing the surface of the resonator (few microns in depth) through subsequent total internal reflections along an equatorial plane. Due to their low material losses and high surface quality, these optical microcavities present an extremely high value of their quality factor Q defined as the ratio between the wavelength λ at which a resonance occurs and the linewidth Δλ of the resonant wavelength. Moreover, their small mode volumes and long storage lifetimes for the photons guarantee high energy density levels and very narrow linewidths for the resonant modes sustained by these

resonant microstructures. All these properties make such optical devices of great interest for applications in lasing, non-linear optics, optical communications and sensing [197–199].

If fused silica represents one of the basic materials for the realisation of WGM microresonators with extremely high Q factor thanks to its excellent chemical durability and transparency in a wide range of wavelengths [200], soft glasses are now gaining an increasing interest as a bulk material for these WGM microcavities due to their better versatility in terms of material properties, low phonon energy, and high rare earth solubility [201–205].

Based on this promising background in terms of materials for WGM microresonators, the basic idea could be to apply ion-exchange process to load the soft glass material constituting these microresonators with noble metal ions and/or nanoparticles in order to create hybrid devices, able to make the most of the intrinsic characteristics of the WGMs joined with those of the ion-exchanged material.

For example, let's consider the case of a lasing emission by up-conversion phenomenon in WGM glass microspheres doped with rare earth ions [206–210]. The possibility to nucleate and grow noble metal nanostructures (i.e.: in the form of dimer clusters and/or metal nanoparticles with few nanometre sizes) within the active medium of the cavity following ion-exchange and thermal post-process may enhance the luminescent efficiency of the rare earth element and its emission by surface plasmon resonance (SPR) and/or energy transfer (ET) mechanisms, as observed for the planar substrates [211–213]. Moreover, an increase in the up-conversion signal comes from the same WGM microcavity which, supporting high recirculating light energy densities, allows the photons to interact several times both with the rare earth ions and metal nanostructures generally located at a distance of few tens/hundreds of nanometres below the cavity surface within the WGMs action field. In particular, if these nanostructures are represented by small plasmonic NPs (e.g., few nanometres in size), then a combination between the two resonant phenomena—the one linked to the host WGM microcavity and the plasmonic one of the nanoparticles—may occur generating a further significant signal enhancement.

Obviously, the ion-exchange process with the consequent presence of noble metal nanostructures may increase the losses in the cavity reducing its Q factor value. In this regard, it should be noted that the thermal annealing process in air may offer a double advantage: formation of noble metal nanoparticles embedded in the glass and smoothening of the WGM microcavity surface as a result of temperature and surface tension. As proof of this statement, K. Milenko and co-workers recently demonstrated how the quality factor Q of a silver iodide phosphate glass microsphere remains almost unchanged ($\sim10^4$) before and after the formation of silver nanoparticles following a thermal annealing treatment in air. The size of silver nanoclusters so obtained was around 350 nm [214]. This encouraging result suggests that the achievement of hybrid WGM microcavities, both in passive and in active glasses, by means of the ion-exchange technique may not be such a distant possibility.

Currently, one of the most promising glass formulations for the realisation of active WGM microresonators is represented by phosphate glasses able to guarantee high Q factor values, above 10^6, for these optical devices both in bulk and coated configuration [201,215]. Hence, these host materials may represent good candidates for the realisation of hybrid active WGM microresonators by ion-exchange process. In this context, it will be mandatory to tailor both the ion-exchange parameters and those of the subsequent post-processing treatment to optimize the size of the noble metal nanostructures (e.g., few nanometres in diameter), minimizing losses in the cavity and keeping the quality factor Q for the resulting hybrid active WGM microcavities as high as possible.

The considerations made above for bulk microspheres continue to be valid also for coated ones such as, for instance, a silica microsphere with a sol-gel thin film coating of compound glass. Applications in the development of visible laser sources for displays should be expected.

The availability of noble metal nanoparticles embedded in a WGM cavity of compound glass could also favour non-linear optical response of the medium that should be further increased by the presence of plasmonic effects. For instance, silver NPs with their large

third order nonlinear properties and optical absorption transitions with high oscillator strengths are the main candidates for the development of all-optical signal processing devices such as efficient optical limiters, which require high nonlinear refractive index n_2 materials [216–218]. Also in this case, the general considerations made previously in terms of the optimisation of both process parameters and quality factor Q are still valid.

It is important to note that, although the plasmonic absorption peak is generally located in the visible region of the spectrum, the absorption band of glasses with embedded silver NPs presents a tail extending to the near infrared region. This suggests how the local field effect induced by SPR phenomenon would have an impact also in this region of the spectrum [159,219]. This would allow to enhance the visible up-conversion emission in erbium doped glasses with embedded silver NPs. The enhancement in the up-conversion intensity may be also attributed to the local field effect induced by the presence of silver NPs [220].

Figure 10 shows a potential up-conversion emission enhancement in the particular case of an Er^{3+}-doped WGM microsphere with embedded silver plasmonic small nanoparticles.
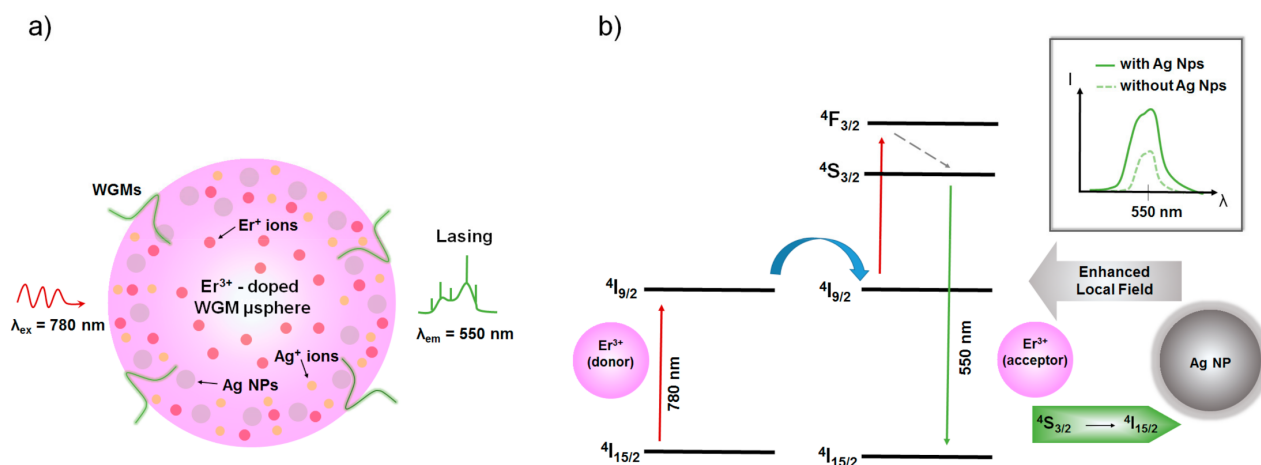

Figure 10. (**a**) Scheme of the up-conversion lasing emission in a Er^{3+}-doped WGM microsphere with embedded silver nanoparticles. (**b**) Potential emission enhancement process in presence of Ag NPs. In the inset, the expected qualitative trend of the erbium up-conversion signal with (continuous line) or without (dashed line) plasmonic silver nanoparticles.

It should also be mentioned here that a further important contribution for the achievement of hybrid WGM microcavities should be offered by the research effort towards the development of novel and efficient glass formulations, suitable for ion-exchange process, with the aim to reduce material absorption losses and scattering effects.

Another noteworthy application of the ion-exchange technique joined with glass WGM microcavity could be represented by growing noble metal NPs (e.g., metal nanoislands or an array of few ordered and equidistant nanoparticles, working as hot spots and based on localized surface plasmon resonance (LSPR) phenomenon), directly on the surface of an ion-exchanged microresonator—in correspondence with its equatorial plane—by means of a thermal post-process performed with laser irradiation. This methodology could represent a valid alternative to the widely used one, which implies the chemical immobilisation of plasmonic nanoparticles on the surface of the resonant microcavity. In comparison to this technique, the strategy based on laser irradiation reduces the processing times and allows to have nanoparticles partially exposed on the surface, therefore more resistant to the various washing steps generally required in biosensing applications. Figure 11 shows the growth mechanism of plasmonic silver nanoparticles on the surface of an ion-exchanged WGM microsphere by laser beam irradiation technique.
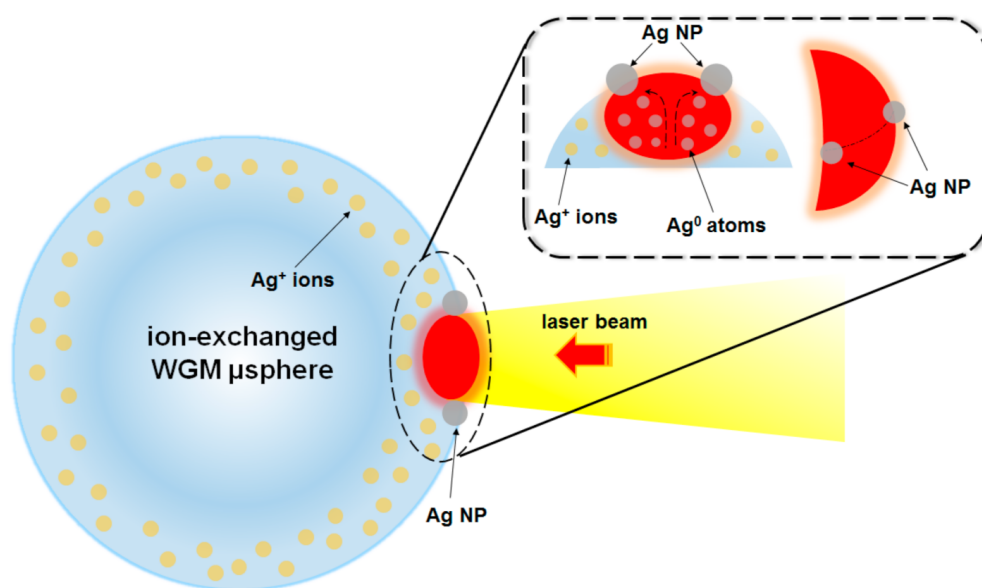
Figure 11. A sketch of the formation mechanism of silver nanoparticles on the WGM microsphere surface by means of a laser beam irradiation. The nanoparticles (NPs) result partially exposed as reported in detail in the inset.

Another strategy to partially expose the noble metal NPs on the surface of a WGM resonant glass microcavity could be represented by a chemical etching step in an extremely dilute solution of hydrofluoric acid (HF), in order to preserve as much as possible a low value of surface roughness for the microresonator.

In recent years, with the improvement of manufacturing techniques, there has been a continuous and growing interest in the realisation of new hybrid optical fibres (HOFs), in which the co-presence within a silica host fibre of multi-materials (e.g., glasses, crystals, semiconductors, etc.) and different guiding structures (e.g., non-linear waveguides, photonic crystals, semiconductor junction, optoelectronic elements, etc.) contributes to broaden their application horizon towards the achievement of an all-fibre photonic platform [221–226]. In this context, ion-exchange in molten salts of noble metals with subsequent thermal post-process may induce the nucleation and growth of plasmon nanoparticles at the end of a possible HOF, whose core is made up of a compound glass suitable for ion-exchange (e.g., silicate, phosphate, tellurite, etc.). Alternatively, the end of a multimode silica optical fibre loaded with a thin layer of soft glass could be used for the same purpose. In the near future, these strategies could represent an effective low-cost solution towards the realisation of optical fibre probes for SERS applications in comparison with current lithographic techniques, such as electron beam lithography (EBL) or nanoimprinting lithography (NIL), surely more effective but definitely complicated and expensive technologies [227,228]. Figure 12 represents some configurations for the development of novel fibre probes for SERS applications. In particular, Figure 12a reports the concept of multimaterial HOF while Figure 12b,c show two possible schemes, one based on HOF and the other on a multimode optical fibre (MOF).

Finally, another application that deserves to be investigated concerns the fabrication of compound glass nanotips [229] with embedded noble metal nanoparticles—following ion-exchange and thermal annealing processes—for SERS and tip enhanced Raman spectroscopy (TERS) applications [230,231].
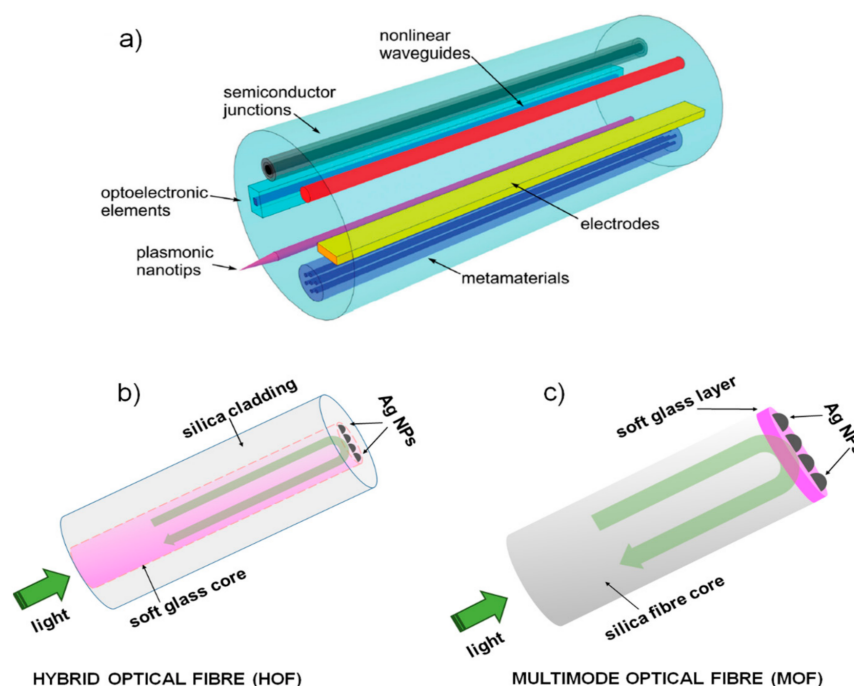
Figure 12. (**a**) The concept of multimaterial hybrid optical fibre (HOF) (figure reprinted from paper [222] under the terms of the Creative Commons Attribution 4.0 International License); (**b**) a possible scheme for a SERS fibre probe based on HOF; (**c**) a possible scheme for SERS fibre probe based on multimode optical fibre (MOF).

5. Conclusions

In this review paper, we have shown how the glass and ion-exchange pair, far from being an obsolete technology, still plays a key role in various technological fields with interesting applications and industrial developments that also have repercussions at the level of everyday life. Moreover, this ancient and indissoluble synergy between material and manufacturing process may lead in the near future to the realisation of new and intriguing photonic devices with further interesting applications in optical communications, non-linear optics, and sensing.

Author Contributions: Conceptualization, S.B.; writing—original draft preparation, review and editing, S.B. and S.P.; supervision, G.C.R. All authors have read and agreed to the published version of the manuscript.

Conflicts of Interest: The authors declare no conflict of interest.

References

1. Rehren, T.; Freestone, I.C. Ancient glass: From kaleidoscope to crystal ball. *J. Archeol. Sci.* **2015**, *56*, 233–241. [CrossRef]
2. Scott, R.B.; Brems, D. The archaeometry of ancient glassmaking: Reconstructing ancient technology and the trade of raw materials. *Perspective* **2014**, *2*, 224–238. [CrossRef]
3. Righini, G.C.; Laybourn, P.J.R. Integrated Optics. In *Perspectives in Optoelectronics*, 1st ed.; Jha, S.S., Ed.; World Scientific Publishing Co. Pte. Ltd.: Singapore; Hackensack, NJ, USA; London, UK; Hong Kong, China, 1995; Chapter 12, pp. 679–736.

4. Righini, G.C.; Pelli, S. Ion-exchange in glass: A mature technology for photonics devices. In Proceedings of the International Symposium on Optical Science and Technology, San Diego, CA, USA, 29 July–3 August 2001; Volume 4453, pp. 93–99. [CrossRef]
5. Pradell, T.; Molera, J.; Roque, J.; Vendrell-Saz, M.; Smith, A.D.; Pantos, E.; Crespo, D. Ionic-exchange mechanism in the formation of medieval luster decorations. *J. Am. Ceram. Soc.* **2005**, *88*, 1281–1289. [CrossRef]
6. Mazzoldi, P.; Sada, C. A trip in the history and evolution of ion-exchange process. *Mat. Sci. Eng. B* **2008**, *149*, 112–117. [CrossRef]
7. Mazzoldi, P.; Carturan, S.; Quaranta, A.; Sada, C.; Sglavo, V.M. Ion-exchange process: History, evolution and applications. *Riv. Nuovo Cim.* **2013**, *36*, 397–460. [CrossRef]
8. Schulze, G. Versuche über die diffusion von silber in glas. *Ann. Phys.* **1913**, *345*, 335–367. [CrossRef]
9. Kistler, S.S. Stresses in glass produced by nonuniform exchange of monovalent Ions. *J. Am. Ceram. Soc.* **1962**, *45*, 59–68. [CrossRef]
10. Acloque, P.; Tochon, J. Measurement of Mechanical Resistance of Glass after Reinforcement. In *Colloquium on Mechanical Strength of Glass and Ways of Improving It*; Union Scientifique Continentale du Verre: Charleroi, Belgium, 1962; Volume 1044, pp. 687–704.
11. Donald, I.W. Methods for improving the mechanical properties of oxide glasses. *J. Mater. Sci.* **1989**, *24*, 4177–4208. [CrossRef]
12. Gy, R. Ion-exchange for glass strengthening. *Mater. Sci. Eng. B* **2008**, *149*, 159–165. [CrossRef]
13. Karlsson, S.; Jonson, B. The technology of chemical glass strengthening—A review. *Glass Technol. Eur. J. Glass Sci. Technol. A* **2010**, *51*, 41–54.
14. Agrawal, G.P. Optical Communication: Its History and Recent Progress. In *Optics in Our Time*; Al-Amri, M., El-Gomati, M., Zubairy, M., Eds.; Springer: Cham, Switzerland, 2016; Chapter 8; pp. 177–199. [CrossRef]
15. Maurer, R.D.; Schultz, P.C. Fused Silica Optical Waveguide. US Patent 365995, 2 May 1972.
16. Keck, D.B.; Schultz, P.C. Method of Producing Optical Waveguide Fibres. US Patent 3711262, 16 January 1973.
17. Miller, S.E. Integrated Optics: An Introduction. *Bell Syst. Tech. J.* **1969**, *48*, 2059–2069. [CrossRef]
18. Izawa, T.; Nakagome, H. Optical waveguide formed by electrically induced migration of ions in glass plates. *Appl. Phys. Lett.* **1972**, *21*, 584–586. [CrossRef]
19. Giallorenzi, T.G.; West, E.J.; Kirk, R.D.; Ginther, R.J.; Andrews, R.A. Optical waveguides formed by thermal migration of ions in glass. *Appl. Opt.* **1973**, *12*, 1240–1245. [CrossRef] [PubMed]
20. Righini, G.C.; Chiappini, A. Glass optical waveguides: A review of fabrication techniques. *Opt. Eng.* **2014**, *53*, 071819. [CrossRef]
21. Thervonen, A.; West, B.R.; Honkanen, S. Ion-exchanged glass waveguide technology: A review. *Opt. Eng.* **2011**, *50*, 071107. [CrossRef]
22. Ramaswamy, R.V.; Srivastava, R. Ion-exchanged glass waveguides: A review. *IEEE J. Light. Technol.* **1988**, *6*, 984–1000. [CrossRef]
23. Honkanen, S.; West, B.R.; Yliniemi, S.; Madasamy, P.; Morrell, M.; Auxier, J.; Schülzgen, A.; Peyghambarian, N.; Carriere, J.; Frantz, J.; et al. Recent advances in ion-exchanged glass waveguides and devices. *Phys. Chem. Glasses: Eur. J. Glass Sci. Technol. B* **2006**, *47*, 110–120.
24. Äyräs, P.; Nunzi Conti, G.; Honkanen, S.; Peyghambarian, N. Birefringence control for ion-exchanged channel glass waveguides. *Appl. Opt.* **1998**, *37*, 8400–8405. [CrossRef]
25. Asquini, R.; D'Angelo, J.; d'Alessandro, A. A Switchable Optical Add-Drop Multiplexer using Ion-Exchange Waveguides and a POLICRYPS Grating Overlayer. *Mol. Cryst. Liq. Cryst.* **2006**, *450*, 203–214. [CrossRef]
26. D'Alessandro, A.; Donisi, D.; De Sio, L.; Beccherelli, R.; Asquini, R.; Caputo, R.; Umeton, C. Tunable integrated optical filter made of a glass ion-exchanged waveguide and an electro-optic composite holographic grating. *Opt. Express* **2008**, *16*, 9254–9260. [CrossRef]
27. Montero-Orille, C.; Moreno, V.; Prieto-Blanco, X.; Mateo, E.F.; Ip, E.; Crespo, J.; Liñares, J. Ion-exchanged glass binary phase plates for mode-division multiplexing. *Appl. Opt.* **2013**, *52*, 2332–2339. [CrossRef]
28. Montero-Orille, C.; Prieto-Blanco, X.; González-Núñez, H.; Liñares, J. A Polygonal Model to Design and Fabricate Ion-Exchanged Diffraction Gratings. *Appl. Sci.* **2021**, *11*, 1500. [CrossRef]
29. Bradley, J.D.B.; Pollnau, M. Erbium-doped integrated waveguide amplifiers and lasers. *Laser Photonics Rev.* **2011**, *5*, 368–403. [CrossRef]
30. Righini, G.C.; Brenci, M.; Forastiere, M.A.; Pelli, S.; Ricci, R.; Nunzi Conti, G.; Peyghambarian, N.; Ferrari, M.; Montagna, M. Rare-earth-doped glasses and ion-exchanged integrated optical amplifiers and lasers. *Phylos. Mag.* **2002**, *82*, 721–734. [CrossRef]
31. Pelli, S.; Bettinelli, M.; Brenci, M.; Calzolai, R.; Chiasera, A.; Ferrari, M.; Nunzi Conti, G.; Speghini, A.; Zampedri, L.; Zheng, J.; et al. Erbium-doped silicate glasses for integrated optical amplifiers and lasers. *J. Non Cryst. Solids* **2004**, *345–346*, 372–376. [CrossRef]
32. Righini, G.C.; Arnaud, C.; Berneschi, S.; Bettinelli, M.; Brenci, M.; Chiasera, A.; Feron, P.; Ferrari, M.; Montagna, M.; Nunzi Conti, G.; et al. Integrated optical amplifiers and microspherical lasers based on erbium-doped oxide glasses. *Opt. Mater.* **2005**, *27*, 1711–1717. [CrossRef]
33. Berneschi, S.; Bettinelli, M.; Brenci, M.; Dall'Igna, R.; Nunzi Conti, G.; Pelli, S.; Profilo, B.; Sebastiani, S.; Speghini, A.; Righini, G.C. Optical and spectroscopic properties of soda-lime alumino silicate glasses doped with Er^{3+} and/or Yb^{3+}. *Opt. Mater.* **2006**, *28*, 1271–1275. [CrossRef]
34. Ondráček, F.; Jágerská, J.; Salavcová, L.; Míka, M.; Špirková, J.; Čtyroký, J. Er–Yb Waveguide Amplifiers in Novel Silicate Glasses. *IEEE J. Quantum Electron.* **2008**, *44*, 536–541. [CrossRef]
35. Laporta, P.; Taccheo, S.; Longhi, S.; Svelto, O.; Svelto, C. Erbium–ytterbium microlasers: Optical properties and lasing characteristics. *Opt. Mater.* **1999**, *11*, 269–288. [CrossRef]

36. Della Valle, G.; Taccheo, S.; Sorbello, G.; Cianci, E.; Foglietti, V.; Laporta, P. Compact high gain erbium-ytterbium doped waveguide amplifier fabricated by Ag-Na ion-exchange. *Electron. Lett.* **2006**, *42*, 632–633. [CrossRef]

37. Jaouën, Y.; du Mouza, L.; Barbier, D.; Delavaux, J.-M.; Bruno, P. Eight-Wavelength Er–Yb Doped Amplifier: Combiner/Splitter Planar Integrated Module. *IEEE Photonics Technol. Lett.* **1999**, *11*, 1105–1107. [CrossRef]

38. Conzone, S.; Hayden, J.S.; Funk, D.S.; Roshko, A.; Veasey, D.L. Hybrid glass substrates for waveguide device manufacture. *Opt. Lett.* **2001**, *26*, 509–511. [CrossRef]

39. Yliniemi, S.; Albert, J.; Wang, Q.; Honkanen, S. UV-exposed Bragg gratings for laser applications in silver-sodium phosphate glass waveguides. *Opt. Express* **2006**, *14*, 2898–2903. [CrossRef] [PubMed]

40. Molina, G.; Murica, S.; Molera, J.; Roldan, C.; Crespo, D.; Pradell, T. Color and dichroism of silver-stained glasses. *J. Nanopart. Res.* **2013**, *15*, 1932–1937. [CrossRef]

41. Puche-Roig, A.; Martín, V.P.; Murcia- Mascarós, S.; Ibáñez Puchades, R. Float glass colouring by ion-exchange. *J. Cult. Herit.* **2008**, *9*, e129–e133. [CrossRef]

42. Berg, K.-J.; Berger, K.A.; Hofmeister, H. Small silver particles in glass surface layers produced by sodium-silver ion-exchange—their concentration and size depth profile. *Z. Phys. D At. Mol. Clust.* **1991**, *20*, 309–311. [CrossRef]

43. Berger, A. Concentration and size depth profile of colloidal silver particles in glass surface produced by sodium-silver ion-exchange. *J. Non Cryst. Solids* **1992**, *151*, 88–94. [CrossRef]

44. Manikandan, D.; Mohan, S.; Magudapathy, P.; Nair, K.G.M. Blue shift of plasmon resonance in Cu and Ag ion-exchanged and annealed soda-lime glass: An optical absorption study. *Phys. B Condens. Matter.* **2003**, *325*, 86–91. [CrossRef]

45. Quaranta, A.; Rahman, A.; Mariotto, G.; Maurizio, C.; Trave, E.; Gonella, F.; Cattaruzza, E.; Gibaudo, E.; Broquin, J.E. Spectroscopic Investigation of Structural Rearrangements in Silver Ion-Exchanged Silicate Glasses. *J. Phys. Chem. C* **2012**, *116*, 3757–3764. [CrossRef]

46. Mohapatra, S. Tunable surface plasmon resonance of silver nanoclusters in ion-exchanged soda lime glass. *J. Alloys Compd.* **2014**, *598*, 11–15. [CrossRef]

47. Madrigal, J.B.; Tellez-Limon, R.; Gardillou, F.; Barbier, D.; Geng, W.; Couteau, C.; Salas-Montiel, R.; Blaize, S. Hybrid integrated optical waveguides in glass for enhanced visible photoluminescence of nanoemitters. *Appl. Opt.* **2016**, *55*, 10263–10268. [CrossRef] [PubMed]

48. Ashley, P.R.; Bloemer, M.J.; Davis, J.H. Measurement of nonlinear properties in Ag-ion-exchange waveguides using degenerate four-wave mixing. *Appl. Phys. Lett.* **1990**, *57*, 1488–1490. [CrossRef]

49. Faccio, D.; Trapani, D.P.; Borsella, E.; Gonella, F.; Mazzoldi, P.; Malvezzi, A.M. Measurement of the third-order nonlinear susceptibility of Ag nanoparticles in glass in a wide spectral range. *Europhys. Lett.* **1998**, *43*, 213–218. [CrossRef]

50. Tagantsev, D.K.; Kazansky, P.G.; Lipovskii, A.A.; Maluev, K.D. Ion-exchange-induced formation of glassy electrooptical and nonlinear optical nanomaterial. *J. Non Cryst. Solids* **2008**, *354*, 1369–1372. [CrossRef]

51. Karvonen, L.; Rönn, J.; Kujala, S.; Chen, Y.; Säynätjoki, A.; Tervonen, A.; Svirko, Y.; Honkanen, S. High non-resonant third-order optical nonlinearity of Ag–glass nanocomposite fabricated by two-step ion-exchange. *Opt. Mater.* **2013**, *36*, 328–332. [CrossRef]

52. Xiang, W.; Gao, H.; Ma, L.; Ma, X.; Huang, Y.; Pei, L.; Liang, X. Valence State Control and Third-Order Nonlinear Optical Properties of Copper Embedded in Sodium Borosilicate Glass. *ACS Appl. Mater. Interfaces* **2015**, *7*, 10162–10168. [CrossRef] [PubMed]

53. Kumar, P.; Mathpal, M.C.; Hamad, S.; Rao, S.V.; Neethling, J.H.; Janse, A.; van Vuuren, A.J.; Njoroge, E.G.; Kroon, R.E.; Roos, W.D.; et al. Cu nanoclusters in ion-exchanged soda-lime glass: Study of SPR and nonlinear optical behavior for photonics. *Appl. Mater. Today* **2019**, *15*, 323–334. [CrossRef]

54. Malta, O.; Santa-Cruz, P.A.; de Sa´, G.F.; Auzel, F. Fluorescence enhancement induced by the presence of small silver particles in Eu^{3+} doped materials. *J. Lumin.* **1985**, *33*, 261–272. [CrossRef]

55. Hayakawa, T.; Selvan, S.T.; Nogami, M. Field enhancement effect of small Ag particles on the fluorescence from Eu^{3+}-doped SiO$_2$ glass. *Appl. Phys. Lett.* **1999**, *74*, 1513–1515. [CrossRef]

56. Strohhöfer, C.; Polman, A. Silver as a sensitizer for erbium. *Appl. Phys. Lett.* **2002**, *81*, 1414–1416. [CrossRef]

57. Chiasera, A.; Ferrari, M.; Mattarelli, M.; Montagna, M.; Pelli, S.; Portales, H.; Zheng, J.; Righini, G.C. Assessment of spectroscopic properties of erbium ions in a soda-lime silicate glass after silver–sodium exchange. *Opt. Mater.* **2005**, *27*, 1743–1747. [CrossRef]

58. Mattarelli, M.; Montagna, M.; Vishnubhatla, K.; Chiasera, A.; Ferrari, M.; Righini, G.C. Mechanisms of Ag to Er energy transfer in silicate glasses: A photoluminescence study. *Phys. Rev. B* **2007**, *75*, 125102. [CrossRef]

59. Li, L.; Yang, Y.; Zhou, D.; Yang, Z.; Xu, X.; Qiu, J. Investigation of the role of silver species on spectroscopic features of Sm^{3+}-activated sodium aluminosilicate glasses via Ag$^+$-Na$^+$ ion-exchange. *J. Appl. Phys.* **2013**, *113*, 193103. [CrossRef]

60. Li, L.; Yang, Y.; Zhou, D.; Yang, Z.; Xu, X.; Qiu, J. Investigation of the interaction between different types of Ag species and europium ions in Ag$^+$-Na$^+$ ion-exchange glass. *Opt. Mater. Express* **2013**, *3*, 806–812. [CrossRef]

61. Gonella, F. Silver doping glasses. *Ceram. Int.* **2015**, *41*, 6693–6701. [CrossRef]

62. Stanek, S.; Nekvindova, P.; Svecova, B.; Vytykacova, S.; Mika, M.; Oswald, J.; Barkman, O.; Spirkova, J. The influence of silver ion-exchange on the luminescence properties of Er-Yb silicate glasses. *Opt. Mater.* **2017**, *72*, 183–189. [CrossRef]

63. Zhao, J.; Yang, Z.; Yu, C.; Qiu, J.; Song, Z. Preparation of ultra-small molecule-like Ag nano-clusters in silicate glass based on ion-exchange process: Energy transfer investigation from molecule-like Ag nano-clusters to Eu^{3+} ions. *Chem. Eng. J.* **2018**, *341*, 175–186. [CrossRef]

64. Zhao, J.; Zhu, J.; Yang, Z.; Jiao, Q.; Yu, C.; Qiu, J.; Song, Z. Selective preparation of Ag species on photoluminescence of Sm^{3+} in borosilicate glass via Ag^+-Na^+ ion-exchange. *J. Am. Ceram. Soc.* **2019**, *103*, 955–964. [CrossRef]

65. Mironov, L.Y.; Sgibnev, Y.M.; Kolesnikov, I.E.; Nikonorov, N.V. Luminescence and energy transfer mechanisms in photo-thermo-refractive glasses co-doped with silver molecular clusters and Eu^{3+}. *Phys. Chem. Chem. Phys.* **2020**, *22*, 23342–23350. [CrossRef]

66. Sgibnev, Y.; Asamoah, B.; Nikonorov, N.; Honkanen, S. Tunable photoluminescence of silver molecular clusters formed in Na^+-Ag^+ ion-exchanged antimony-doped photo-thermo-refractive glass matrix. *J. Lumin.* **2020**, *226*, 117411. [CrossRef]

67. Allsopp, B.L.; Orman, R.; Johnson, S.R.; Baistow, I.; Sanderson, G.; Sundberg, P.; Stålhandske, C.; Grund, L.; Andersson, A.; Booth, J.; et al. Towards improved cover glasses for photovoltaic devices. *Prog. Photovolt. Res. Appl.* **2020**, *28*, 1187–1206. [CrossRef]

68. Huang, X.; Han, S.; Huang, W.; Liu, X. Enhancing solar cell efficiency: The search for luminescent materials as spectral converters. *Chem. Soc. Rev.* **2013**, *42*, 173–201. [CrossRef] [PubMed]

69. Cattaruzza, E.; Mardegan, M.; Pregnolato, T.; Ungaretti, G.; Aquilanti, G.; Quaranta, A.; Battaglin, G.; Trave, E. Ion-exchange doping of solar cell coverglass for sunlight down-shifting. *Sol. Energy Mater. Sol. Cells* **2014**, *130*, 272–280. [CrossRef]

70. Cattaruzza, E.; Caselli, V.M.; Mardegan, M.; Gonella, F.; Bottaro, G.; Quaranta, A.; Valotto, G.; Enrichi, F. $Ag^+ \leftrightarrow Na^+$ ion-exchanged silicate glasses for solar cells covering: Down-shifting properties. *Ceram. Int.* **2015**, *41*, 7221–7226. [CrossRef]

71. Mardegan, M.; Cattaruzza, E. Cu-doped photovoltaic glasses by ion-exchange for sunlight down–shifting. *Opt. Mater.* **2016**, *61*, 105–110. [CrossRef]

72. Li, Y.; Chen, F.; Liu, C.; Han, J.; Zhao, X. UV–Visible spectral conversion of silver ion-exchanged aluminosilicate glasses. *J. Non-Cryst. Solids* **2017**, *471*, 82–90. [CrossRef]

73. Enrichi, F.; Armellini, C.; Battaglin, G.; Belluomo, F.; Belmokhtar, S.; Bouajaj, A.; Cattaruzza, E.; Ferrari, M.; Gonella, F.; Lukowiak, A.; et al. Silver doping of silica-hafnia waveguides containing Tb^{3+}/Yb^{3+} rare earths for down conversion in PV solar cells. *Opt. Mater.* **2016**, *60*, 264–269. [CrossRef]

74. Sgibnev, Y.; Cattaruzza, E.; Dubrovin, V.; Vasilyev, V.; Nikonorov, N. Photo-Thermo-Refractive Glasses Doped with Silver Molecular Clusters as Luminescence Downshifting Material for Photovoltaic Applications. *Part. Part. Syst. Charact.* **2018**, *35*, 1800141. [CrossRef]

75. Bubli, I.; Ali, S.; Ali, M.; Hayat, K.; Iqbal, Y.; Zulfiqar, S.; ul Haq, A.; Cattaruzza, E. Enhancement of solar cell efficiency via luminescent downshifting by an optimized coverglass. *Ceram. Int.* **2020**, *46*, 2110–2115. [CrossRef]

76. Enrichi, F.; Belmokhtar, S.; Benedetti, A.; Bouajaj, A.; Cattaruzza, E.; Coccetti, F.; Colusso, E.; Ferrari, M.; Ghamgosar, P.; Gonella, F.; et al. Ag nanoaggregates as efficient broadband sensitizers for Tb^{3+} ions in silica-zirconia ion-exchanged sol-gel glasses and glass-ceramics. *Opt. Mater.* **2018**, *84*, 668–674. [CrossRef]

77. Tresnakova, P.; Malichova, H.; Spirkova, J.; Mika, M. Fabrication of optical layers containing Er(III) and Cu(I) in silicate glasses. *J. Phys. Chem. Solids* **2007**, *68*, 1276–1279. [CrossRef]

78. Yu, C.; Zhao, J.; Zhu, J.; Huang, A.; Qiu, J.; Song, Z.; Zhou, D. Luminescence enhancement and white light generation of Eu^{3+} and Dy^{3+} single-doped and co-doped tellurite glasses by Ag nanoparticles based on Ag^+-Na^+ ion-exchange. *J. Alloys Compd.* **2018**, *748*, 717–729. [CrossRef]

79. Tang, L.; Chen, N. White light emitting YVO_4:Eu^{3+},Tm^{3+},Dy^{3+} nanometer- and submicrometer-sized particles prepared by an ion-exchange method. *Ceram. Int.* **2016**, *42*, 302–309. [CrossRef]

80. Sgibnev, Y.M.; Nikonorov, N.V.; Ignatiev, A.I. Luminescence of silver clusters in ion-exchanged cerium-doped photo-thermo-refractive glasses. *J. Lumin.* **2016**, *176*, 292–297. [CrossRef]

81. Sgibnev, Y.M.; Nikonorov, N.V.; Ignatiev, A.I. High efficient luminescence of silver clusters in ion-exchanged antimony doped photo-thermo-refractive glasses: Influence of antimony content and heat treatment parameters. *J. Lumin.* **2017**, *188*, 172–179. [CrossRef]

82. Zhou, Y.; Laybourn, P.J.R.; Magill, J.V.; De La Rue, R.M. An evanescent fluorescence biosensor using ion-exchanged buried waveguides and the enhancement of peak fluorescence. *Biosens. Bioelectron.* **1991**, *6*, 595–607. [CrossRef]

83. Zhou, Y.; Magill, J.V.; De La Rue, R.M.; Laybourn, P.J.R. Evanescent fluorescence immunoassays performed with a disposable ion-exchanged patterned waveguide. *Sens. Actuators B Chem.* **1993**, *11*, 245–250. [CrossRef]

84. Srivastava, R.; Bao, C.; Gómez-Reino, C. Planar-surface waveguide evanescent-wave chemical sensors. *Sens. Actuators A Phys.* **1996**, *51*, 165–171. [CrossRef]

85. Hassanzadeh, A.; Nitsche, M.; Mittler, S.; Armstrong, S.; Dixon, S.J.; Langbein, U. Waveguide evanescent field fluorescence microscopy: Thin film fluorescence intensities and its application in cell biology. *Appl. Phys. Lett.* **2008**, *92*, 233503. [CrossRef]

86. Hassanzadeh, A.; Nitsche, M.; Armstrong, S.; Nabavi, N.; Harrison, R.; Dixon, S.J.; Langbein, U. Optical waveguides formed by silver ion-exchange in Schott SG11 glass for waveguide evanescent field fluorescence microscopy: Evanescent images of HEK293 cells. *J. Biomed. Opt.* **2010**, *15*, 036018. [CrossRef]

87. Araci, I.E.; Mendes, S.B.; Yurt, N.; Honkanen, S.; Peyghambarian, N. Highly sensitive spectroscopic detection of heme-protein sub-monolayer films by channel integrated optical waveguide. *Opt. Express* **2007**, *15*, 5595–5603. [CrossRef] [PubMed]

88. Karabchevsky, A.; Kavokin, A.V. Giant absorption of light by molecular vibrations on a chip. *Sci. Rep.* **2016**, *6*, 21201. [CrossRef]

89. Zhu, M.; Kari, N.; Yan, Y.; Yimit, A. The fabrication and gas sensing application of a fast-responding m-CP-PVP composite film/potassium ion-exchanged glass optical waveguide. *Anal. Methods* **2017**, *9*, 5494–5501. [CrossRef]

90. Du, B.; Tong, Z.; Mu, X.; Xu, J.; Liu, S.; Liu, Z.; Cao, W.; Qi, Z.-M. A Potassium Ion-Exchanged Glass Optical Waveguide Sensor Locally Coated with a Crystal Violet-SiO2 Gel Film for Real-Time Detection of Organophosphorus Pesticides Simulant. *Sensors* **2019**, *19*, 4219. [CrossRef] [PubMed]

91. Homola, J.; Čtyroký, J.; Skalský, M.; Hradilová, J.; Kolářová, J.P. A surface plasmon resonance based integrated optical sensor. *Sens. Actuators B Chem.* **1997**, *39*, 286–290. [CrossRef]

92. Dostálek, J.; Čtyroký, J.; Homola, J.; Brynda, E.; Skalský, M.; Nekvindová, P.; Špirková, J.; Škvor, J.; Schröfel, J. Surface plasmon resonance biosensor based on integrated optical waveguide. *Sens. Actuators B Chem.* **2001**, *76*, 8–12. [CrossRef]

93. De Bonnault, S.; Bucci, D.; Zermatten, P.J.; Charette, P.G.; Broquin, J.E. Hybrid metallic ion-exchanged waveguides for SPR biological sensing. In Proceedings of the SPIE, San Francisco, CA, USA, 7–12 February 2015; Volume 9365, p. 93650. [CrossRef]

94. Tellez-Limon, R.; Gardillou, F.; Coello, V.; Salas-Montiel, R. Coupled localized surface plasmon resonances in periodic arrays of gold nanowires on ion-exchange waveguide technology. *J. Opt.* **2021**, *23*, 25801. [CrossRef]

95. Nashchekin, A.V.; Nevedomskiy, V.N.; Obraztsov, P.A.; Stepanenko, O.V.; Sidorov, A.I.; Usov, O.A.; Turoverov, K.K.; Konnikov, S.G. Waveguide-type localized plasmon resonance biosensor for noninvasive glucose concentration detection. In Proceedings of the SPIE, Brussels, Belgium, 16–19 April 2012; Volume 8427, p. 842739. [CrossRef]

96. Pilot, R.; Signorini, R.; Durante, C.; Orian, L.; Bhamidipati, M.; Fabris, L. A Review on Surface-Enhanced Raman Scattering. *Biosensors* **2019**, *9*, 57. [CrossRef] [PubMed]

97. Mosier-Boss, P.A. Review of SERS Substrates for Chemical Sensing. *Nanomaterials* **2017**, *7*, 142. [CrossRef]

98. Zhang, J.; Dong, W.; Sheng, J.; Zheng, J.; Li, J.; Qiao, L.; Jiang, L. Silver nanoclusters formation in ion-exchanged glasses by thermal annealing, UV-laser and X-ray irradiation. *J. Non Cryst. Solids* **2008**, *310*, 234–239. [CrossRef]

99. Kolobkova, E.; Sergeevna Kuznetsova, M.; Nikonorov, N. Ag/Na Ion-exchange in Fluorophosphate Glasses and Formation of Ag Nanoparticles in the Bulk and on the Surface of the Glass. *ACS Appl. Nano Mater.* **2019**, *2*, 6928–6938. [CrossRef]

100. Karvonen, L.; Chen, Y.; Säynätjoki, A.; Taiviola, K.; Tervonen, A.; Honkanen, S. SERS-active silver nanoparticle aggregates produced in high-iron float glass by ion-exchange process. *Opt. Mater.* **2011**, *34*, 1–5. [CrossRef]

101. Babich, E.; Kaasik, V.; Redkov, A.; Maurer, T.; Lipovskii, A. SERS-Active Pattern in Silver-Ion-Exchange Glass Drawn by Infrared Nanosecond Laser. *Nanomaterials* **2020**, *10*, 1849. [CrossRef] [PubMed]

102. Tite, T.; Ollier, N.; Sow, M.C.; Vocanson, F.; Goutaland, F. Ag nanoparticles in soda-lime glass grown by continuous wave laser irradiation as an efficient SERS platform for pesticides detection. *Sens. Actuators B Chem.* **2017**, *242*, 127–131. [CrossRef]

103. Chen, Y.; Jaakola, J.; Ge, Y.; Säynätjoki, A.; Tervonen, A.; Hannula, S.-P.; Honkanen, S. In situ fabrication of waveguide-compatible glass-embedded silver nanoparticle patterns by masked ion-exchange process. *J. Non Cryst. Solids* **2009**, *355*, 2224–2227. [CrossRef]

104. Chen, Y.; Jaakola, J.; Säynätjoki, A.; Tervonen, A.; Honkanen, S. Glass-embedded silver nanoparticle patterns by masked ion-exchange process for surface-enhanced Raman scattering. *J. Raman Spectrosc.* **2011**, *42*, 936–940. [CrossRef]

105. Simo, A.; Joseph, V.; Fenger, R.; Kneipp, J.; Rademann, K. Long-Term Stable Silver Subsurface Ion-Exchanged Glasses for SERS Applications. *Chem. Phys. Chem.* **2011**, *12*, 1683–1688. [CrossRef]

106. Simo, A.; Polte, J.; Pfänder, N.; Vainio, U.; Emmerling, F.; Rademann, K. Formation Mechanism of Silver Nanoparticles Stabilized in Glassy Matrices. *J. Am. Chem. Soc.* **2012**, *134*, 18824–18833. [CrossRef]

107. Hofmeister, H.; Tan, G.L.; Dubiel, M. Shape and internal structure of silver nanoparticles embedded in glass. *J. Mater. Res.* **2005**, *20*, 1551–1562. [CrossRef]

108. Williams, T. *The Glass Menagerie*, 1st ed.; Random House Publisher: New York, NY, USA, 1945.

109. Chesterton, G.K. *Orthodoxy*, 1st ed.; John Lane/Bodley Head Publisher: London, UK, 1909.

110. Varshneya, A.K. Chemical Strengthening of Glass: Lessons Learned and Yet to Be Learned. Int. *J. Appl. Glass Sci.* **2010**, *1*, 131–142. [CrossRef]

111. Romaniuk, R.S. Tensile strength of tailored optical fibres. *Opto Electron. Rev.* **2000**, *8*, 101–116.

112. Wisitsorasak, A.; Wolynes, P. On the strength of glasses. *PNAS* **2012**, *109*, 16068–16072. [CrossRef] [PubMed]

113. Nielsen, J.H.; Bjarrum, M. Deformations and strain energy in fragments of tempered glass: Experimental and numerical investigation. *Glass Struct. Eng.* **2017**, *2*, 133–146. [CrossRef]

114. Datsiou, K.C.; Overend, M. The strength of aged glass. *Glass Struct. Eng.* **2017**, *2*, 105–120. [CrossRef]

115. Gardon, R. Thermal tempering of glass. In *Glass Science and Technology. Elasticity and Strength in Glasses*; Uhlmann, D.R., Kreidl, N.J., Eds.; Academic Press: New York, NY, USA, 1980; Volume 5, pp. 145–216. [CrossRef]

116. Sglavo, V.M.; Quaranta, A.; Allodi, V.; Mariotto, G. Analysis of surface structure of soda lime silicate glasses after chemical strengthening in different KNO_3 salt bath. *J. Non Cryst. Solids* **2014**, *401*, 105–109. [CrossRef]

117. Mognato, E.; Schiavonato, M.; Barbieri, A.; Pittoni, M. Process influences on mechanical strength of chemical strengthened glass. *Glass Struct. Eng.* **2016**, *1*, 247–260. [CrossRef]

118. Rogoziński, R. Stresses Produced in the BK7 Glass by the K^+–Na^+ Ion-exchange: Real-Time Process Control Method. *Appl. Sci.* **2019**, *9*, 2548. [CrossRef]

119. Cooper, A.R.; Krohn, D.A. Strengthening of glass fibres II: Ion-exchange. *J. Am. Ceram. Soc.* **1969**, *52*, 665–669. [CrossRef]

120. Dugnani, R. Residual stress in ion-exchanged silicate glass: An analytical solution. *J. Non Cryst. Solids* **2017**, *471*, 368–378. [CrossRef]

121. Varshneya, A.K. The physics of chemical strengthening of glass: Room for a new view. *J. Non Cryst. Solids* **2010**, *356*, 2289–2294. [CrossRef]

122. Macrelli, G. Chemically strengthened glass by ion-exchange: Strength evaluation. *Int. J. Appl. Glass Sci.* **2017**, *9*, 156–166. [CrossRef]
123. Macrelli, G.; Varshneya, A.K.; Mauro, J.C. Simulation of glass network evolution during chemical strengthening: Resolution of the subsurface compression maximum anomaly. *J. Non Cryst. Solids* **2019**, *552*, 119457. [CrossRef]
124. Macrelli, G.; Özben, N.; Kayaalp, A.C.; Ersundu, M.C.; Sökmen, I. Stress in ion-exchanged soda-lime silicate and sodium aluminosilicate glasses: Experimental and theoretical comparison. *Int. J. Appl. Glass Sci.* **2020**, *11*, 730–742. [CrossRef]
125. Terakado, N.; Sasaki, R.; Takahashi, Y.; Fujiwara, T.; Orihara, S.; Orihara, Y. A novel method for stress evaluation in chemically strengthened glass based on micro-Raman spectroscopy. *Commun. Phys.* **2020**, *3*, 1–7. [CrossRef]
126. Erdem, I.; Guldiren, D.; Aydin, S. Chemical tempering of soda lime silicate glasses by ion-exchange process for the improvement of surface and bulk mechanical strength. *J. Non Cryst. Solids* **2017**, *473*, 170–178. [CrossRef]
127. Aaldenberg, E.M.; Lezzi, P.J.; Seaman, J.H.; Blanchet, T.A.; Tomozawa, M. Ion-Exchanged Lithium Aluminosilicate Glass: Strength and Dynamic Fatigue. *J. Am. Ceram. Soc.* **2016**, *99*, 2645–2654. [CrossRef]
128. Li, X.; Jiang, L.; Wang, Y.; Mohagheghian, I.; Dear, J.P.; Ki, L.; Yan, Y. Correlation between K^+-Na^+ diffusion coefficient and flexural strength of chemically tempered aluminosilicate glass. *J. Non Cryst. Solids* **2017**, *47*, 72–81. [CrossRef]
129. Ragoen, C.; Sen, S.; Lambricht, T.; Godet, S. Effect of Al2O3 content on the mechanical and interdiffusional properties of ion-exchanged Na-aluminosilicate glasses. *J. Non Cryst. Solids* **2017**, *458*, 129–136. [CrossRef]
130. Available online: https://www.corning.com/microsites/csm/gorillaglass/PI_Sheets/2020/Corning%20Gorilla%20Glass%20 6_PI%20Sheet.pdf (accessed on 17 May 2021).
131. Available online: https://photonicsolutioncenter.com/media/companies/133/products/439/documents/agc-dragontrail-chemically.pdf (accessed on 17 May 2021).
132. Available online: https://www.schott.com/d/xensation/7d59e8ca-a167-4d23-b375-6a8040cc9eb6/1.0/schott-xensation-up-datasheet-english-row-20052019.pdf (accessed on 17 May 2021).
133. Available online: https://abrisatechnologies.com/specs/SCHOTT%20Xensation%20Spec%20Sheet.pdf#zoom=100 (accessed on 17 May 2021).
134. Wilson, J.R.; Jones, C.D.; Bartlow, C.C.; Doan, A.R. Patterned Asymmetric Chemical Strengthening. US Patent 20200017406A1, 16 January 2020.
135. Luzzato, V.; Prest, C.D.; Memering, D.N.; Rogers, M.S. Asymmetric Chemical Strengthening. US Patent 20170334769A1, 23 November 2017.
136. Rogers, M.S.; Memering, D.N.; Prest, C.D. Asymmetric Chemical Strengthening. US Patent 20150274585A1, 1 October 2015.
137. Available online: https://www.corning.com/microsites/csm/gorillaglass/PI_Sheets/2020/Corning%20Gorilla%20Glass%20 Victus_PI%20Sheet.pdf (accessed on 17 May 2021).
138. Available online: https://www.apple.com/iphone-12/ (accessed on 17 May 2021).
139. Available online: https://media.ford.com/content/fordmedia/fna/us/en/news/2015/12/15/industry-first-gorilla-glass-hybrid-windshield-on-all-new-ford-GT.html (accessed on 17 May 2021).
140. Available online: https://phys.org/news/2015-12-gorilla-glass-cell-cars.html (accessed on 17 May 2021).
141. Wang, H.F.; Xing, G.Z.; Wang, X.Y.; Zhang, L.L.; Zhang, L.; Li, S. Chemically strengthened protection glasses for the applications of space solar cells. *AIP Adv.* **2014**, *4*, 47133. [CrossRef]
142. Kambe, M.; Hara, K.; Mitarai, K.; Takeda, S.; Fukawa, M.; Ishimaru, N.; Kondo, M. Chemically strengthened cover glass for preventing potential induced degradation of crystalline silicon solar cells. In Proceedings of the 39th Photovoltaic Specialists Conference, Tampa Bay, FL, USA, 16–21 June 2013. [CrossRef]
143. Li, J.; Wei, R.; Liu, X.; Guo, H. Enhanced luminescence via energy transfer from Ag^+ to RE ions (Dy^{3+}, Sm^{3+}, Tb^{3+}) in glasses. *Opt. Express* **2012**, *20*, 10122–10127. [CrossRef]
144. Jiao, Q.; Wang, X.; Qiu, J.; Zhou, D. Effect of silver ions and clusters on the luminescence properties of Eu-doped borate glasses. *Mater. Res. Bull.* **2015**, *72*, 264–268. [CrossRef]
145. Li, L.; Yang, Y.; Zhou, D.; Xu, X.; Qiu, J. The influence of Ag species on spectroscopic features of Tb^{3+}-activated sodium–aluminosilicate glasses via Ag^+–Na^+ ion exchange. *J. Non Cryst. Solids* **2014**, *385*, 95–99. [CrossRef]
146. Bozelli, J.C.; de Oliveira Nunes, L.A.; Sigoli, F.A.; Mazali, I.O. Erbium and Ytterbium Codoped Titanoniobophosphate Glasses for Ion-Exchange-Based Planar Waveguides. *J. Am. Ceram. Soc.* **2010**, *93*, 2689–2692. [CrossRef]
147. Vařák, P.; Vytykáčová, S.; Nekvindová, P.; Michalcová, A.; Malinský, P. The influence of copper and silver in various oxidation states on the photoluminescence of Ho^{3+}/Yb^{3+} doped zinc-silicate glasses. *Opt. Mater.* **2019**, *91*, 253–260. [CrossRef]
148. He, X.; Xu, X.; Shi, Y.; Qiu, J. Effective enhancement of Bi near-infrared luminescence in silicogermanate glasses via silver–sodium ion exchange. *J. Non Cryst. Solids* **2015**, *409*, 178–182. [CrossRef]
149. Paje, S.E.; García, M.A.; Villegas, M.A.; Llopis, J. Cerium doped soda-lime-silicate glasses: Effects of silver ion-exchange on optical properties. *Opt. Mater.* **2001**, *17*, 459–469. [CrossRef]
150. Grand, J.; Lamy de la Chapelle, M.; Bijeon, J.-L.; Adam, P.-M.; Vial, A.; Royer, P. Role of localized surface plasmons in surface-enhanced Raman scattering of shape-controlled metallic particles in regular arrays. *Phys. Rev. B* **2005**, *72*, 033407. [CrossRef]
151. Li, P.; Long, F.; Chen, W.; Chen, J.; Chu, P.K.; Wang, H. Fundamentals and applications of surface-enhanced Raman spectroscopy-based biosensors. *Curr. Opin. Biomed. Eng.* **2020**, *13*, 51–59. [CrossRef]

152. Betz, J.F.; Yu, W.W.; Cheng, Y.; White, I.M.; Rubloff, G.W. Simple SERS substrates: Powerful, portable, and full of potential. *PCCP* **2014**, *16*, 2224–2239. [CrossRef]

153. Fan, M.; Andrade, G.F.S.; Brolo, A.G. A review on the fabrication of substrates for surface enhanced Raman spectroscopy and their applications in analytical chemistry. *Anal. Chim. Acta* **2011**, *693*, 7–25. [CrossRef] [PubMed]

154. Zhao, J.; Lin, J.; Zhang, W.; Wei, H.; Chen, Y. SERS-active Ag nanoparticles embedded in glass prepared by a two-step electric field-assisted diffusion. *Opt. Mater.* **2014**, *39*, 97–102. [CrossRef]

155. Chen, Y.; Jaakola, J.; Säynätjoki, A.; Tervonen, A.; Honkanen, S. SERS-active silver nanoparticles in ion-exchanged glass. *J. Nonlinear Opt. Phys.* **2010**, *19*, 527–533. [CrossRef]

156. Manikandan, P.; Manikandan, D.; Manikandan, E.; Christy Ferdinand, A. Surface enhanced Raman scattering (SERS) of silver ions embedded nanocomposite glass. *Spectrochim. Acta A Mol. Biomol. Spectrosc.* **2014**, *124*, 203–207. [CrossRef]

157. Manikandan, P.; Manikandan, D.; Manikandan, E.; Christy Ferdinand, A. Structural, Optical and Micro-Raman Scattering Studies of Nanosized Copper Ion (Cu+) Exchanged Soda Lime Glasses. *Plasmonics* **2014**, *9*, 637–643. [CrossRef]

158. Quaranta, A.; Cattaruzza, E.; Gonella, F.; Rahman, A.; Mariotto, G. Cross-sectional Raman micro-spectroscopy study of silver nanoparticles in soda–lime glasses. *J. Non Cryst. Solids* **2014**, *401*, 219–223. [CrossRef]

159. Chen, Y.; Karvonen, L.; Säynätjoki, A.; Ye, C.; Tervonen, A.; Honkanen, S. Ag nanoparticles embedded in glass by two-step ion exchange and their SERS application. *Opt. Mater. Express* **2011**, *1*, 164–172. [CrossRef]

160. Manzani, D.; Franco, D.F.; Afonso, C.R.M.; Sant'Ana, A.C.; Nalih, M.; Ribeiro, S.J.L. A new SERS substrate based on niobium lead-pyrophosphate glasses obtained by Ag$^+$/Na$^+$ ion exchange. *Sens. Actuators B Chem.* **2018**, *277*, 347–352. [CrossRef]

161. De Marchi, G.; Caccavale, F.; Gonella, F.; Mattei, G.; Mazzoldi, P.; Battaglin, G.; Quaranta, A. Silver nanoclusters formation in ion-exchanged waveguides by annealing in hydrogen atmosphere. *Appl. Phys. A* **1996**, *63*, 403–407. [CrossRef]

162. Redkov, A.V.; Zhurikhina, V.V.; Lipovskii, A.A. Formation and self-arrangement of silver nanoparticles in glass via annealing in hydrogen: The model. *J. Non Cryst. Solids* **2013**, *376*, 152–157. [CrossRef]

163. Chervinskii, S.; Sevriuk, V.; Reduto, I.; Lipovskii, A. Formation and 2D-patterning of silver nanoisland film using thermal poling and out-diffusion from glass. *J. Appl. Phys.* **2013**, *114*, 224301. [CrossRef]

164. Redkov, A.; Chervinskii, S.; Baklanov, A.; Reduto, I.; Zhurikhina, V.; Lipovskii, A. Plasmonic molecules via glass annealing in hydrogen. *Nanoscale Res. Lett.* **2014**, *9*, 606. [CrossRef] [PubMed]

165. Goutaland, F.; Sow, M.; Ollier, N.; Vacanson, F. Growth of highly concentrated silver nanoparticles and nanoholes in silver-exchanged glass by ultraviolet continuous wave laser exposure. *Opt. Mater. Express* **2012**, *2*, 350–357. [CrossRef]

166. Goutaland, F.; Colombier, J.-P.; Cherif Sow, M.; Ollier, N.; Vocanson, F. Laser-induced periodic alignment of Ag nanoparticles in soda-lime glass. *Opt. Express* **2013**, *21*, 31789–31799. [CrossRef]

167. Niry, M.D.; Mostafavi-Amjad, J.; Khalesifard, H.R.; Ahangary, A.; Azizian-Kalandaragh, Y. Formation of silver nanoparticles inside a soda-lime glass matrix in the presence of a high intensity Ar$^+$ laser beam. *J. Appl. Phys.* **2012**, *111*, 033111. [CrossRef]

168. Miotello, A.; Bonelli, M.; De Marchi, G.; Mattei, G.; Mazzoldi, P.; Sada, C.; Gonella, F. Formation of silver nanoclusters by excimer–laser interaction in silver-exchanged soda-lime glass. *Appl. Phys. Lett.* **2001**, *79*, 2456–2458. [CrossRef]

169. Sheng, J.; Zheng, J.; Zhang, J.; Zhou, C.; Jiang, L. UV-laser-induced nanoclusters in silver ion-exchanged soda-lime silicate glass. *Physica B* **2007**, *387*, 32–35. [CrossRef]

170. Wackerow, S.; Abdolvand, A. Laser-assisted one-step fabrication of homogeneous glass–silver composite. *Appl. Phys. A* **2012**, *109*, 45–49. [CrossRef]

171. Wackerow, S.; Abdolvand, A. Generation of silver nanoparticles with controlled size and spatial distribution by pulsed laser irradiation of silver ion-doped glass. *Opt. Express* **2014**, *22*, 5076–5085. [CrossRef]

172. Schmidl, G.; Dellith, J.; Schneidewind, H.; Zopf, D.; Stranik, O.; Gawlik, A.; Anders, S.; Tympel, V.; Katzer, C.; Schmidl, F.; et al. Formation and characterization of silver nanoparticles embedded in optical transparent materials for plasmonic sensor surfaces. *Mater. Sci. Eng. B* **2015**, *193*, 207–216. [CrossRef]

173. Chervinskii, S.; Matikainen, A.; Dergachev, A.; Lipovskii, A.A.; Honkanen, S. Out-diffused silver island films for surface-enhanced Raman scattering protected with TiO$_2$ films using atomic layer deposition. *Nanoscale Res. Lett.* **2014**, *9*, 398. [CrossRef]

174. Inácio, P.L.; Barreto, B.J.; Horowitz, F.; Correia, R.R.B.; Pereira, M.B. Silver migration at the surface of ion-exchange waveguides: A plasmonic template. *Opt. Mater. Express* **2013**, *3*, 390–399. [CrossRef]

175. Hu, J.; Li, L.; Lin, H.; Zhang, P.; Zhou, W.; Ma, Z. Flexible integrated photonics: Where materials, mechanics and optics meet. *Opt. Mater. Express* **2013**, *3*, 1313–1331. [CrossRef]

176. Geiger, S.; Michon, J.; Liu, S.; Qin, J.; Ni, J.; Hu, J.; Gu, T.; Lu, N. Flexible and stretchable Photonics: The Next Stretch of Opportunities. *ACS Photonics* **2020**, *7*, 2618–2635. [CrossRef]

177. Righini, G.C.; Szczurek, A.; Krzak, J.; Lukowiak, A.; Ferrari, M.; Varas, S.; Chiasera, A. Flexible Photonics: Where Are We Now? In Proceedings of the 22nd International Conference on Transparent Optical Networks (ICTON), Bari, Italy, 19–23 July 2020; pp. 1–4. [CrossRef]

178. Righini, G.C.; Krzak, J.; Lukowiak, A.; Macrelli, G.; Varas, S.; Ferrari, M. From flexible electronics to flexible photonics: A brief overview. *Opt. Mater.* **2021**, *115*, 111011. [CrossRef]

179. Sayginer, O.; Iacob, E.; Varas, S.; Szczurek, A.; Ferrari, M.; Lukowiak, A.; Righini, G.C.; Bursi, O.S.; Chiasera, A. Design, fabrication and assessment of an optomechanical sensor for pressure and vibration detection using flexible glass multilayers. *Opt. Mater.* **2021**, *115*, 111023. [CrossRef]

180. Chen, Y.; Li, H.; Li, M. Flexible and tunable silicon photonic circuits on plastic substrates. *Sci. Rep.* **2012**, *2*, 622. [CrossRef]
181. Fan, L.; Varghese, L.T.; Xuan, Y.; Wang, J.; Niu, B.; Qi, M. Direct fabrication of silicon photonic devices on a flexible platform and its application for strain sensing. *Opt. Express* **2012**, *20*, 20564–20575. [CrossRef]
182. Chiasera, A.; Sayginer, O.; Iacob, E.; Szczurek, A.; Varas, S.; Krzak, J.; Bursi, O.S.; Zonta, D.; Lukowiak, A.; Righini, G.C.; et al. Flexible photonics: RF-sputtering fabrication of glass-based systems operating under mechanical deformation conditions. In Proceedings of the SPIE, Strasbourg, France, 29 March–2 April 2020; Volume 11357, p. 1135705. [CrossRef]
183. Li, L.; Lin, H.; Qiao, S.; Zou, Y.; Danto, S.; Richardson, K.; Musgraves, J.D.; Lu, N.; Hu, J. Integrated flexible chalcogenide glass photonic devices. *Nature Photon.* **2014**, *8*, 643–649. [CrossRef]
184. Li, L.; Lin, H.; Qiao, S.; Huang, Y.-H.; Li, J.-Y.; Michon, J.; Gu, T.; Alosno-Ramos, C.; Vivien, L.; Yadav, A.; et al. Monolithically integrated stretchable photonics. *Light Sci. Appl.* **2018**, *7*, 17138. [CrossRef]
185. Li, L.; Lin, H.; Michon, J.; Huang, Y.; Li, J.; Du, Q.; Yadav, A.; Richardson, K.; Gu, T.; Hu, J. A new twist on glass: A brittle material enabling flexible integrated photonics. *Int. J. Appl. Glass Sci.* **2017**, *8*, 61–68. [CrossRef]
186. Lapointe, J.; Ledemi, Y.; Loranger, S.; Iezzi, V.L.; De Lima Filho, E.S.; Parent, F.; Morency, S.; Messaddeq, Y.; Kashyap, R. Fabrication of ultrafast laser written low-loss waveguides in flexible As_2S_3 chalcogenide glass tape. *Opt. Lett.* **2016**, *41*, 203–206. [CrossRef] [PubMed]
187. Available online: https://www.corning.com/worldwide/en/innovation/corning-emerging-innovations/corning-willow-glass.html (accessed on 17 May 2021).
188. Available online: https://www.schott.com/en-gb/products/af-32-eco (accessed on 17 May 2021).
189. Hou, Y.; Cheng, J.; Kang, J.; Cui, J. The forming simulation of flexible glass with silt down draw method. *IOP Conf. Ser.: Mater. Sci. Eng.* **2018**, *324*, 12020. [CrossRef]
190. Garner, S.; Glaesemann, S.; Li, X. Ultra-slim flexible glass for roll-to-roll electronic device fabrication. *Appl. Phys. A* **2014**, *116*, 403–407. [CrossRef]
191. Huang, S.; Li, M.; Garner, S.M.; Li, M.-J.; Chen, K.P. Flexible photonic components in glass substrates. *Opt. Express* **2015**, *23*, 22532–22543. [CrossRef] [PubMed]
192. Ellison, A.; Cornejo, I.A. Glass Substrates for Liquid Crystal Displays. *Int. J. Appl. Glass Sci.* **2010**, *1*, 87–103. [CrossRef]
193. Mauro, J.C.; Truesdale, C.M.; Adib, K.; Whittier, A.M.; Martin, A.W. Chemical Strengthening of Alkali-Free Glass via Pressure Vessel Ion Exchange. *Int. J. Appl. Glass Sci.* **2016**, *7*, 446–451. [CrossRef]
194. Martin, A.W.; Mauro, J.C.; Truesdale, C.M. Strengthened Glass, Glass-Ceramic, and Ceramic Articles and Methods of Making the Same through Pressurized Ion Exchange. U.S. Patent Application 2016/0145152 A1, 2 June 2016.
195. Macrelli, G.; Varshneya, A.K.; Mauro, J.C. Ultra-thin glass as a substrate for flexible photonics. *Opt. Mater.* **2020**, *106*, 109994. [CrossRef]
196. Macrelli, G. Strengthened glass by ion exchange, mechanical and optical properties: Perspectives and limits of glass as a substrate for flexible photonics. In Proceedings of the SPIE Photonics Europe, Strasbourg, France, 29 March–2 April 2020; Volume 11357, p. 1135707. [CrossRef]
197. Chiasera, A.; Dumeige, Y.; Féron, P.; Ferrari, M.; Jestin, Y.; Nunzi Conti, G.; Pelli, S.; Soria, S.; Righini, G.C. Spherical whispering-gallery-mode microresonators. *Laser Photonics Rev.* **2010**, *4*, 457–482. [CrossRef]
198. Ward, J.; Benson, O. WGM microresonators: Sensing, lasing and fundamental optics with microspheres. *Laser Photonics Rev.* **2011**, *5*, 553–570. [CrossRef]
199. Strekalov, D.V.; Marquardt, C.; Matsko, A.B.; Schwefel, H.G.L.; Leuchs, G. Nonlinear and quantum optics with whispering gallery resonators. *J. Opt.* **2016**, *18*, 18–123002. [CrossRef]
200. Gorodetsky, M.L.; Savchenkov, A.A.; Ilchenko, V.S. Ultimate Q of optical microsphere resonators. *Opt. Lett.* **1996**, *21*, 453–455. [CrossRef]
201. Ristić, D.; Berneschi, S.; Camerini, M.; Farnesi, D.; Pelli, S.; Trono, C.; Chiappini, A.; Chiasera, A.; Ferrari, M.; Lukowiak, A.; et al. Photoluminescence and lasing in whispering gallery mode glass microspherical resonators. *J. Lumin.* **2016**, *170*, 755–760. [CrossRef]
202. Ward, J.M.; Yang, Y.; Nic Chormaic, S. Glass-on-glass fabrication of bottle-shaped tunable microlasers and their applications. *Sci. Rep.* **2016**, *6*, 25152. [CrossRef] [PubMed]
203. Yu, J.; Lewis, E.; Farrell, G.; Wang, P. Compound glass microsphere resonator devices. *Micromachines* **2018**, *9*, 356. [CrossRef] [PubMed]
204. Zhu, J.; Zohrabi, M.; Bae, K.; Horning, T.M.; Grayson, M.B.; Park, W.; Gopinath, J.T. Nonlinear characterization of silica and chalcogenide microresonators. *Optica* **2019**, *6*, 716–722. [CrossRef]
205. Yu, J.; Zhang, J.; Wang, R.; LI, A.; Zhang, M.; Wang, S.; Wang, P.; Ward, J.M.; Nic Chormaic, S. A tellurite glass optical microbubble resonator. *Opt. Express* **2020**, *28*, 32858–32868. [CrossRef] [PubMed]
206. Fujiwara, H.; Sasaki, K. Up-conversion lasing of a thulium-ion-doped fluorozirconate glass microsphere. *J. Appl. Phys.* **1999**, *86*, 2385–2388. [CrossRef]
207. Von Klitzing, W.; Jahier, E.; Long, R.; Lissillour, F.; Lefèvre-Seguin, V.; Hare, J.; Raimond, J.-M.; Haroche, S. Very low threshold green lasing in microspheres by up-conversion of IR photons. *J. Opt. B Quantum Semiclass. Opt.* **2000**, *2*, 204–206. [CrossRef]
208. Wu, Y.; Ward, J.M.; Nic Chormaic, S. Ultralow threshold green lasing and optical bistability in ZBNA (ZrF_4–BaF_2–NaF–AlF_3) microspheres. *J. Appl. Phys.* **2010**, 33103. [CrossRef]

209. Wang, X.; Yu, Y.; Wang, S.; Ward, J.M.; Nic Chormaic, S.; Wang, P. Single mode green lasing and multicolour luminescent emission from an Er^{3+}-Yb^{3+} co-doped compound fluorosilicate glass microsphere resonator. *OSA Contin.* **2018**, *1*, 261–273. [CrossRef]

210. Huang, Y.; Zhuang, S.; Peng, L.; Wu, J.; Liao, T.; Xu, C.; Duan, Y. Efficiency improvement of up-conversion luminescence of Yb^{3+}/Tm^{3+} co-doped tellurite glass microsphere. *J. Alloys Compd.* **2018**, *748*, 93–99. [CrossRef]

211. Singh, S.K.; Giri, N.K.; Rai, D.K.; Rai, S.B. Enhanced up-conversion emission in Er^{3+}-doped tellurite glass containing silver nanoparticles. *Solid State Sci.* **2010**, *12*, 1480–1483. [CrossRef]

212. Reza Dousti, M. Efficient infrared-to-visible up-conversion emission in Nd^{3+}-doped PbO-TeO$_2$ glass containing silver nanoparticles. *J. Appl. Phys.* **2013**, *114*, 113105. [CrossRef]

213. Soltani, I.; Hraiech, S.; Horchani-Naifer, K.; Férid, M. Effects of silver nanoparticles on the enhancement of up-conversion and infrared emission in Er^{3+}/Yb^{3+} co-doped phosphate glasses. *Opt. Mater.* **2018**, *77*, 161–169. [CrossRef]

214. Milenko, K.; Konidakis, I.; Pissadakis, S. Silver iodide phosphate glass microsphere resonator integrated on an optical fiber taper. *Opt. Lett.* **2016**, *41*, 2185–2188. [CrossRef]

215. Dong, C.H.; Yang, Y.; Shen, Y.L.; Zou, C.L.; Sun, F.W.; Ming, H.; Guo, G.C.; Han, Z.F. Observation of microlaser with Er-doped phosphate glass coated microsphere pumped by 780 nm. *Opt. Commun.* **2010**, *283*, 5117–5120. [CrossRef]

216. Mai, H.H.; Kaydashev, V.E.; Tikhomirov, V.K.; Janssens, E.; Shestakov, M.V.; Meledina, M.; Turner, S.; Van Tendeloo, G.; Moshchalkov, V.V.; Lievens, P. Nonlinear Optical Properties of Ag Nanoclusters and Nanoparticles Dispersed in a Glass Host. *J. Phys. Chem. C* **2014**, *118*, 15995–16002. [CrossRef]

217. Adamiv, V.T.; Bolesta, Y.V.; Gamernyk, R.V.; Karbovnyk, I.D.; Kolych, I.I.; Kovalchuk, M.G.; Kushnir, O.O.; Periv, M.V.; Teslyuk, I.M. Nonlinear optical properties of silver nanoparticles prepared in Ag doped borate glasses. *Physica B* **2014**, *449*, 31–35. [CrossRef]

218. Ferrari, P.; Upadhyay, S.; Shestakov, M.V.; Vanbuel, J.; De Roo, B.; Kuang, Y.; Di Vece, M.; Moshchalkov, V.V.; Locquet, J.-P.; Lievens, P.; et al. Wavelength-Dependent Nonlinear Optical Properties of Ag Nanoparticles Dispersed in a Glass Host. *J. Phys. Chem. C* **2017**, *121*, 27580–27589. [CrossRef]

219. Chen, F.; Cheng, J.; Dai, S.; Xu, Z.; Ji, W.; Tan, R.; Zhang, Q. Third-order optical nonlinearity at 800 and 1300 nm in bismuthate glasses doped with silver nanoparticles. *Opt. Express* **2014**, *22*, 13438–13447. [CrossRef]

220. Amjad, R.J.; Sahar, M.R.; Ghoshal, S.K.; Dousti, M.R.; Riaz, S.; Tahir, B.A. Enhanced infrared to visible upconversion emission in Er^{3+} doped phosphate glass: Role of silver nanoparticles. *J. Lumin.* **2012**, *132*, 2714–2718. [CrossRef]

221. Konidakis, I.; Zito, G. Pissadakis, S. Silver plasmon resonance effects in AgPO$_3$/silica photonic bandgap fiber. *Opt. Lett.* **2014**, *39*, 3374–3377. [CrossRef] [PubMed]

222. Schmidt, M.A.; Argyros, A.; Sorin, F. Hybrid Optical Fibers—An Innovative Platform for In-Fiber Photonic Devices. *Adv. Optical Mater.* **2016**, *4*, 13–36. [CrossRef]

223. Jain, C.; Rodrigues, B.P.; Wieduwilt, T.; Kobelke, J.; Wondraczek, L.; Schmidt, M.A. Silver metaphosphate glass wires inside silica fibers—a new approach for hybrid optical fibers. *Opt. Express* **2016**, *24*, 3258–3267. [CrossRef] [PubMed]

224. Ballato, J.; Peacock, A.C. Perspective: Molten core optical fiber fabrication—A route to new materials and applications. *APL Photonics* **2018**, *3*, 120903. [CrossRef]

225. Kang, S.; Dong, G.; Qiu, J.; Yang, Z. Hybrid glass optical fibers-novel fiber materials for optoelectronic application. *Opt. Mater. X* **2020**, *6*, 100051. [CrossRef]

226. Ballato, J.; Dragic, P.D. Glass: The carrier of light—Part II—A brief look into the future of optical fiber. *Int. J. Appl. Glass Sci.* **2021**, *12*, 3–24. [CrossRef]

227. Pisco, M.; Cusano, A. Lab-On-Fiber Technology: A Roadmap toward Multifunctional Plug and Play Platforms. *Sensors* **2020**, *20*, 4705. [CrossRef]

228. Kostovski, G.; White, D.J.; Mitchell, A.; Austin, M.W.; Stoddart, P.R. Nanoimprinted optical fibres: Biotemplated nanostructures for SERS sensing. *Biosens. Bioelectron.* **2009**, *24*, 1531–1535. [CrossRef]

229. Barucci, A.; Cosi, F.; Giannetti, A.; Pelli, S.; Griffini, D.; Insinna, M.; Salvadori, S.; Tiribilli, B.; Righini, G.C. Optical fibre nanotips fabricated by a dynamic chemical etching for sensing applications. *J. Appl. Phys.* **2015**, *117*, 053104. [CrossRef]

230. Hutter, T.; Elliott, S.R.; Mahajan, S. Optical fibre-tip probes for SERS: Numerical study for design considerations. *Opt. Express* **2018**, *26*, 15539–15550. [CrossRef] [PubMed]

231. Lu, F.; Huang, T.; Han, L.; Su, H.; Wang, H.; Liu, M.; Zhang, W.; Wang, X.; Mei, T. Tip-Enhanced Raman Spectroscopy with High-Order Fiber Vector Beam Excitation. *Sensors* **2018**, *18*, 3841. [CrossRef] [PubMed]